

Jurassic volcanic and sedimentary rocks of the La Silla and Todos Santos Formations, Chiapas: Record of Nazas arc magmatism and rift-basin formation prior to opening of the Gulf of Mexico

Antonio Godínez-Urban¹, Timothy F. Lawton², Roberto S. Molina Garza³, Alexander Iriondo³, Bodo Weber⁴, and Margarita López-Martínez⁴

¹Posgrado en Ciencias de la Tierra, Universidad Nacional Autónoma de México, Campus Juriquilla, Querétaro, Mexico

²Department of Geological Sciences, New Mexico State University, Las Cruces, New Mexico, USA

³Centro de Geociencias, Universidad Nacional Autónoma de México, Campus Juriquilla, Querétaro, Mexico

⁴División de Ciencias de la Tierra, CICESE (Centro de Investigación Científica y de Educación Superior de Ensenada), Ensenada, Baja California, Mexico

ABSTRACT

Stratigraphic relationships, detrital zircon provenance, U-Pb and $^{40}\text{Ar}/^{39}\text{Ar}$ geochronology, and trace element geochemistry in volcanic and sedimentary rocks of the Sierra homocline of central Chiapas near La Angostura reservoir in Mexico document an extensive pulse of Early–Middle Jurassic arc magmatism in rocks that overlie and intrude the Permian–Triassic Chiapas massif. Upper Jurassic rift-basin strata unconformably overlie the volcanic rocks and the massif. A Pliensbachian U-Pb (zircon) SHRIMP (sensitive high-resolution ion microprobe) age from porphyritic andesite (191.0 ± 3.0 Ma), Early to Middle Jurassic $^{40}\text{Ar}/^{39}\text{Ar}$ dates from andesitic dikes, U-Pb grain ages of detrital zircons in overlying strata (196–161 Ma), and previously reported K-Ar dates indicate that subduction-related magmatism occurred in the western portion of the Maya block from Early to latest Middle Jurassic time. We assign the volcanic rocks to the La Silla Formation, which correlates with the informal Pueblo Viejo andesite of the Cintalapa and Uzpanapa regions to the northwest. La Silla magmatism predates opening of the Gulf of Mexico Basin. The Todos Santos Formation, which overlies La Silla Formation, was deposited in extensional basins during the early stages of gulf opening. We recognize a lower El Diamante Member of the Todos Santos, consisting of red fluvial sandstone, mudstone, and minor conglomerate containing primarily volcanic-lithic detritus; this member is characterized by a nearly unimodal Jurassic detrital zircon age population that indicates a Callovian or younger

depositional age. Volcanic activity continued into the upper part of the El Diamante Member, but with a more mafic character. We also recognize an upper member, which we term the Jericó Member. This member is characterized by thickly bedded, coarse-grained pebbly arkose intercalated with several thick intervals (tens of meters) of conglomerate and pebbly sandstone. Sandstone petrology indicates a source in the granitic rocks of the Chiapas massif, with a tendency to show deep-seated sources and a diverse zircon population in the upper part of the section. The upper Todos Santos Formation in the study area is gradational into the overlying San Ricardo Formation (Kimmeridgian–Tithonian). The La Silla Formation was deposited in volcanic-complex environments, with a clear lack of differentiated volcanic rocks. Fluvial strata of the El Diamante Member were deposited in a mud-rich sinuous river system. The Jericó Member was deposited in large, sand-rich fluvial systems, which probably represent deposits of rift-axis trunk streams; conglomerate facies were deposited in adjacent and interfingering alluvial fan systems. We suggest that the stratigraphic record of the western Maya block records a transition from volcanic arc to intra-arc basin and subsequently to rift basin during Pliensbachian to Oxfordian time.

INTRODUCTION

The Gulf of Mexico is best interpreted as a subsidiary basin to the Atlantic Ocean (Pindell et al., 2006). Most models suggest that the Gulf of Mexico Basin formed after the central Atlantic, and invoke origin of the gulf basin

by continental rifting, sea-floor spreading, and associated counterclockwise rotation of the Maya (or Yucatan) block in the Late Jurassic (Pindell and Dewey, 1982; Ross and Scotese, 1988; Dickinson and Lawton, 2001; Bird et al., 2005). These models are based on geometric and plate kinematic constraints such as the reconstruction of western equatorial Pangea and the drift history of South America (Pindell and Dewey, 1982; Pindell et al., 1988), the Jurassic stratigraphy of the gulf and northeastern Mexico (e.g., Winker and Buffler, 1988; Salvador, 1987; Goldhammer, 1999), the tectonic fabric of the deep gulf (Scott and Peel, 2001), and paleomagnetic data (Molina-Garza et al., 1992; Guerrero et al., 1990).

Other details of the reconstruction of the Maya block in the northern Gulf of Mexico region are less well constrained. For example, the Chiapas massif can be reconstructed in the Río Grande embayment or in the Burgos Basin prior to opening of the Gulf of Mexico. Similarly, the orientation of the continental rift basins that preceded opening of the gulf is uncertain and somewhat controversial (Salvador, 1987; Pindell et al., 2006; Exxon, 1985). The rotation of the Maya block assumes an Euler pole in the general region between the Florida peninsula and southern Cuba (e.g., Hall and Najmuddin, 1994; Marton and Buffler, 1994). Estimates of the amount of rotation range between $\sim 30^\circ$ and 60° . Rotation was accommodated by the Tamaulipas-Chiapas transform, along the gulf coast region of the states of Tamaulipas and Veracruz.

The role of arc magmatism in northern Mexico, represented by the Nazas Formation, in the geodynamic context of opening of the Gulf of Mexico has seldom been explored in

the literature despite the fact that arc volcanic rocks are spatially associated with rift successions (Fastovsky et al., 2005; Barboza-Gudiño, 2008). The Gulf of Mexico was recently interpreted as a backarc basin as a result of inferred association with Jurassic Nazas magmatism (Stern and Dickinson, 2009, 2010).

In order to better constrain the tectonic setting of the Maya block prior to opening of the Gulf of Mexico, we integrate geochronologic, stratigraphic, and detrital zircon provenance data for the Todos Santos Formation and underlying volcanic rocks (La Silla Formation) in central Chiapas. Reconstruction of the Chiapas massif offshore of Tamaulipas in Early Jurassic time indicates that the Nazas and La Silla Formations are part of the same arc system, and that the overlying Todos Santos Formation records rift-basin extension immediately following cessation of arc magmatism. These data, together with reappraisal of the relevant circum-gulf Jurassic geology, leads us to the conclusion that the Middle–Late Jurassic rift basins of the Gulf of Mexico region evolved as successors of intra-arc extensional basins of the central Mexico Nazas arc.

REGIONAL SETTING

Basement

Basement of the Maya block includes the Permian–Triassic metamorphic and plutonic complex of the Chiapas massif (Weber et al., 2005), Silurian plutons (Steiner and Walker, 1996), inferred Pan-African rocks buried beneath Mesozoic strata (Krogh et al., 1993; Keppie et al., 2010), and Grenville basement such as the Guichicovi Complex (Weber and Köhler, 1999). Igneous rocks of the Chiapas massif are dominated by Late Permian ages, but have significant Grenville age zircon inheritance (1.02–1.05 Ga; Weber et al., 2005). Contemporaneous medium- to high-grade metamorphism affected Paleozoic sedimentary rocks and Early Permian igneous rocks (Weber et al., 2007). The massif is a Permian–Triassic batholithic complex that represents the record of subduction under western equatorial Pangea; the associated arc can be reconstructed from scattered outcrops of Permian calc-alkaline plutons across northern Mexico from Sonora (Arvizu et al., 2009) to Las Delicias in Coahuila (McKee et al., 1988), from drill-core data eastward in the Tampico area and the Santa Ana high of the Tuxpan–Poza Rica region (Torres-Vargas et al., 1999), and from outcrops in northern Oaxaca (Solari et al., 2001). The arc was called the East Mexico arc by Dickinson and Lawton (2001), but it is not restricted to eastern Mexico.

Todos Santos Formation

Prior to this study, the nonmarine Todos Santos Formation was the oldest Mesozoic unit recognized in the Maya block. It was deposited in extensional basins during the early stages of continental rifting in the Gulf of Mexico region (Fig. 1). Elsewhere in Mexico, similar lithologies have been assigned to the Huizachal Formation (Mixon et al., 1959). Some confusion exists in the literature because the name Todos Santos has been applied to continental redbeds and other terrigenous sequences across southern Mexico (Chiapas and Oaxaca), Guatemala, and Honduras; the name thus applies to Jurassic and Cretaceous strata in different tectonic settings and in different basins (e.g., Burkart et al., 1973; Blair, 1987; Rueda-Gaxiola, 1998; Gose and Finch, 1992).

Clemons et al. (1974) assigned a Late Jurassic–Early Cretaceous age to Todos Santos strata in Guatemala, at the type locality in the Altos Cuchumatanes. However, in rocks overlying the Chiapas massif, Jurassic K-Ar ages (from 196 ± 3 to 148 ± 6 Ma) have been reported near Cintalapa for intermediate volcanic rocks, which were interpreted as part of the Todos Santos succession (Castro-Mora et al., 1975; Herrera-Soto and Estavillo-González, 1991). If Todos Santos strata in Chiapas were indeed Late Jurassic–Early Cretaceous in age, as is the case in Guatemala, these rocks could not be related to the early stages of continental rifting in the gulf. The rifting event is of Early–Middle Jurassic age in northeastern Mexico (Fastovsky et al., 2005). Moreover, the presence of Middle Jurassic calc-alkaline volcanic rocks in the Todos Santos Formation is not entirely consistent with a continental rift setting.

Near Cintalapa, the Todos Santos Formation is overlain by the San Ricardo Formation (Fig. 2), a transitional to shallow-marine succession of sandstone, shale, and marly limestone that contains a Kimmeridgian–Portlandian (Tithonian) fauna (Alencaster, 1977). The contact between the upper Todos Santos and lower San Ricardo Formations has been interpreted as transitional, and the units interfinger in the subsurface with marine evaporites (Viniegra-Osorio, 1971) that likely predate development of oceanic crust in the Gulf of Mexico Basin. In the Isthmus of Tehuantepec, the Todos Santos Formation is overlain by the Upper Jurassic Mogoñe Formation (Herrera-Soto and Estavillo-González, 1991). Pérez-Gutiérrez et al. (2009) reported pre-Jurassic maximum depositional ages of ca. 228 Ma on the basis of detrital zircon young grain ages from Todos Santos strata near Matías Romero, Oaxaca, in the Tehuantepec region.

The Todos Santos Formation in Chiapas consists of polymictic conglomerate, sandstone, mudstone, volcanic rocks, and volcanoclastic deposits. These rocks were deposited in alluvial fans, fluvial systems, and lacustrine environments, forming vertically stacked cyclic megasequences hundreds of meters in thickness; Blair (1987) reported a thickness of 250–1350 m for this unit. The formation unconformably overlies rocks of the Chiapas massif and upper Paleozoic strata in the Chicomuselo uplift (Anderson et al., 1973; Castro-Mora et al., 1975; López-Ramos, 1981), suggesting deposition on irregular topography formed by extensional tectonics (Meneses-Rocha, 1985; Blair, 1987). There are excellent exposures of Todos Santos strata in the Sierra homocline province of west-central Chiapas (Fig. 3). The following section summarizes our observations and mapping, the basis for proposing a new stratigraphic scheme for this region.

METHODS

This work is based in photointerpretation and field mapping at a scale 1:25,000 of an area ~ 700 km 2 in the Sierra homocline of west-central Chiapas, centered near the village of Independencia (Fig. 4). This work is supplemented by reconnaissance description of key stratigraphic columns, petrography (from which we obtained modal compositions), and sampling for U-Pb geochronology, trace element geochemistry, and Ar-Ar dating.

We collected three sandstone samples for detrital zircon provenance analysis. We processed ~ 3 kg of sample using magnetic separation and standard heavy-liquid methods at UNAM (Universidad Nacional Autónoma de México) Centro de Geociencias mineral separation laboratory. A large fraction of the zircon separates was mounted in epoxy resin and polished. Zircons were analyzed in a Micromass Isoprobe multicollector-inductively coupled plasma–mass spectrometer (ICP-MS) at the University of Arizona. The analytical procedure and errors were described in Gehrels et al. (2008). We utilized the GSA 2009 geologic time scale (Walker and Geissman, 2009).

Nine volcanic samples of the La Silla Formation and one of the El Diamante Member of the Todos Santos Formation were analyzed for trace elements using an ICP-MS at the Centro de Geociencias, UNAM, following the methodology described by Mori et al. (2007). In addition, zircons were obtained from andesite from site VC-4 ($X = 510297$, $Y = 1780092$; Universal Transverse Mercator, UTM Zone 15Q), after crushing using standard magnetic separation and heavy liquids. U-Pb analyses

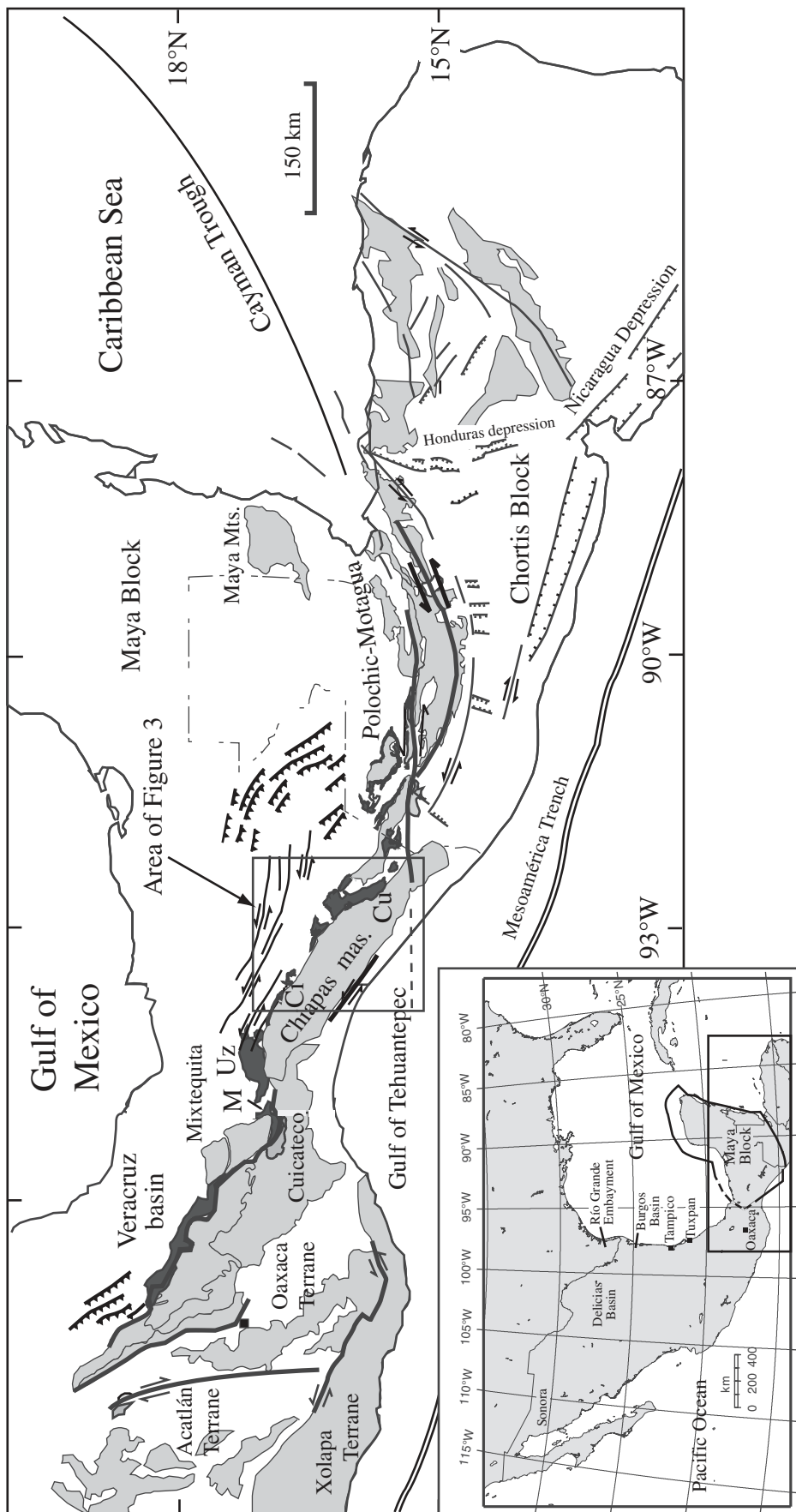


Figure 1. Crystalline rocks of southern Mexico and Central America (light gray), terranes, and outcrop belt of the Todos Santos Formation (dark gray). Some localities mentioned in the text: Ci—Cintalapa, Cu—Cuicatlapan, M—Matías Romero, Uz—Upanapa.

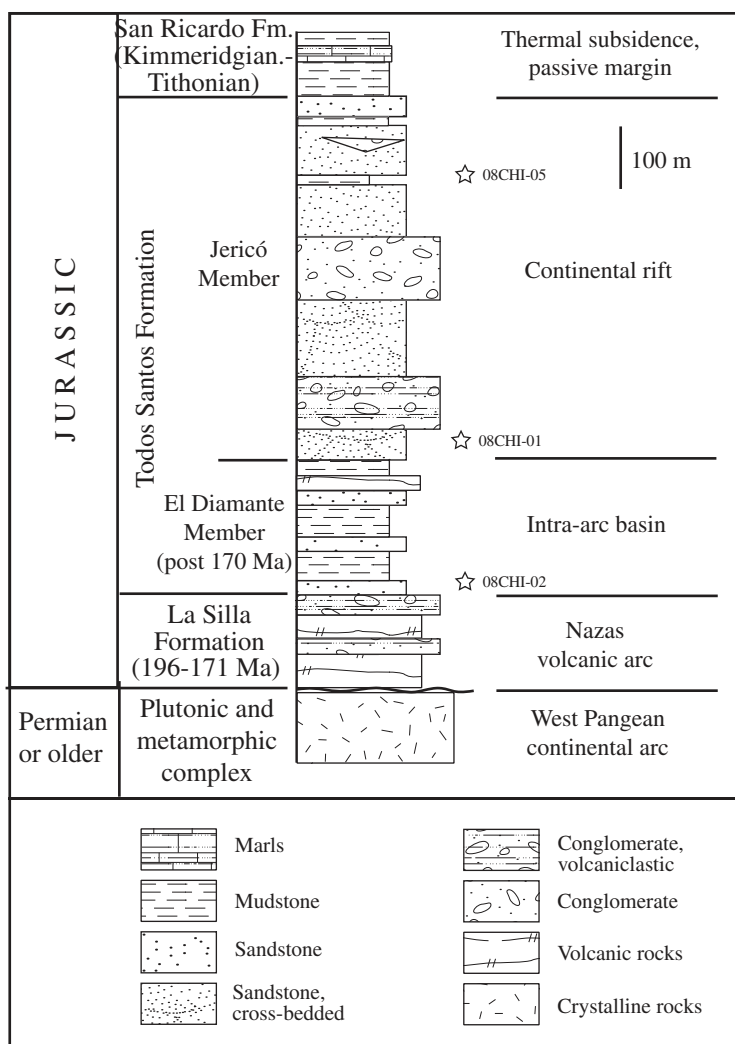


Figure 2. Stratigraphic column of the Sierra homocline of west-central Chiapas, with sampling levels for detrital zircon.

were obtained at Stanford University using a SHRIMP-RG instrument (sensitive high-resolution ion microprobe–reverse geometry; see Nourse et al., 2005, for analytical techniques). Additional geochronology was obtained from samples that were analyzed at the $^{40}\text{Ar}/^{39}\text{Ar}$ facility of CICESE (Centro de Investigación Científica y de Educación Superior de Ensenada), following the technique described in Cerca-Martínez et al. (2000). The aphanitic character of the rocks permits only whole-rock analysis, except in one case.

REVISED STRATIGRAPHY OF THE TODOS SANTOS FORMATION

In the Sierra homocline of Chiapas (Fig. 3), we recognize a lower volcanic and volcanioclastic succession and two younger, predominantly

sedimentary, nonmarine assemblages assigned to the Todos Santos Formation. We term the volcanic succession, which nonconformably overlies rocks of the Chiapas massif, the La Silla Formation and correlate it with the informal Pueblo Viejo andesite near Cintalapa (Castro-Mora et al., 1975). The Todos Santos Formation in places overlies rocks of the Chiapas massif on a nonconformity and elsewhere unconformably overlies La Silla Formation (Fig. 2).

The La Silla Formation consists of abundant intermediate volcanic, hypabyssal, and volcanioclastic rocks and subordinate sandstone, conglomerate, and mudstone. Volcanic rocks in the mapped region crop out in the mountains near the village of El Diamante. We designate a type locality 3 km north of the village of El Diamante at Cerro La Silla (Fig. 4). The volcanic rocks (Fig. 5A) include porphyritic

andesite with plagioclase, hornblende, and pyroxene phenocrysts in a gray, red, or purple aphanitic groundmass. Also common are aphanitic basaltic andesites, which are commonly vesicular to amygdaloidal, with vesicles filled by zeolite or quartz. More evolved rocks such as dacites are common, but rhyolitic compositions are uncommon. Tuffs and pyroclastic rocks are also present, suggesting subaerial emplacement. Pyroclastic rocks include possible block and ash flows and lahars. The lower depositional contact of the volcanic assemblage, where it overlies foliated granitoids, is irregular and rocks both above and below the contact are strongly altered.

Conglomeratic sandstone and mudstone are interbedded with volcanic rocks, but the volcanic succession at La Silla is overlain by a dominantly sedimentary succession with uncommon volcanic rocks. Sedimentary rocks that unconformably overlie the La Silla Formation include the stratigraphically lowest part of the Todos Santos Formation and are assigned to a lower member, the El Diamante Member. This member is mostly composed of red sandstone and mudstone (Fig. 5B). Scour and fill structures, small-scale trough cross-beds, mud drapes, and rip-up clasts are typical; sandstone bodies are lenticular, and form the bases of several-meter-thick upward-fining cycles capped by mudstone, which is commonly pedogenically modified. Sandstone beds are 10–90 cm thick, but the succession is dominated by mudstone, which makes up 60%–80% of the member. The ratio of mudstone to sandstone is ~6:1. The outcrops of this member are characterized by low topography due to the low resistance of the fine fraction to erosion.

A second volcanic interval occurs high in the El Diamante Member, and is characterized by isolated flows of olivine basalt. The contact between the volcanic La Silla assemblage and the overlying lower member of the Todos Santos Formation is a subtle angular unconformity. Fluvial sandstones fill topography developed in the volcanic facies. The lower Todos Santos member is also characterized by its red color and the marked abundance of volcanic detritus.

The upper member of the Todos Santos Formation, the Jericó Member, consists of coarse-grained arkosic and pebbly sandstone beds 0.5–5 m thick, with common large-scale trough cross-beds, horizontal lamination, and boulder lags at bed bases (Fig. 5D). The contact between the El Diamante Member and the overlying Jericó Member is transitional or an erosional surface.

Intercalated within the arkosic Jericó Member are several thick (tens of meters) intervals of conglomerate and pebbly sandstone (Fig. 5C). In this region, Blair (1987) recognized megasequences composed of four main

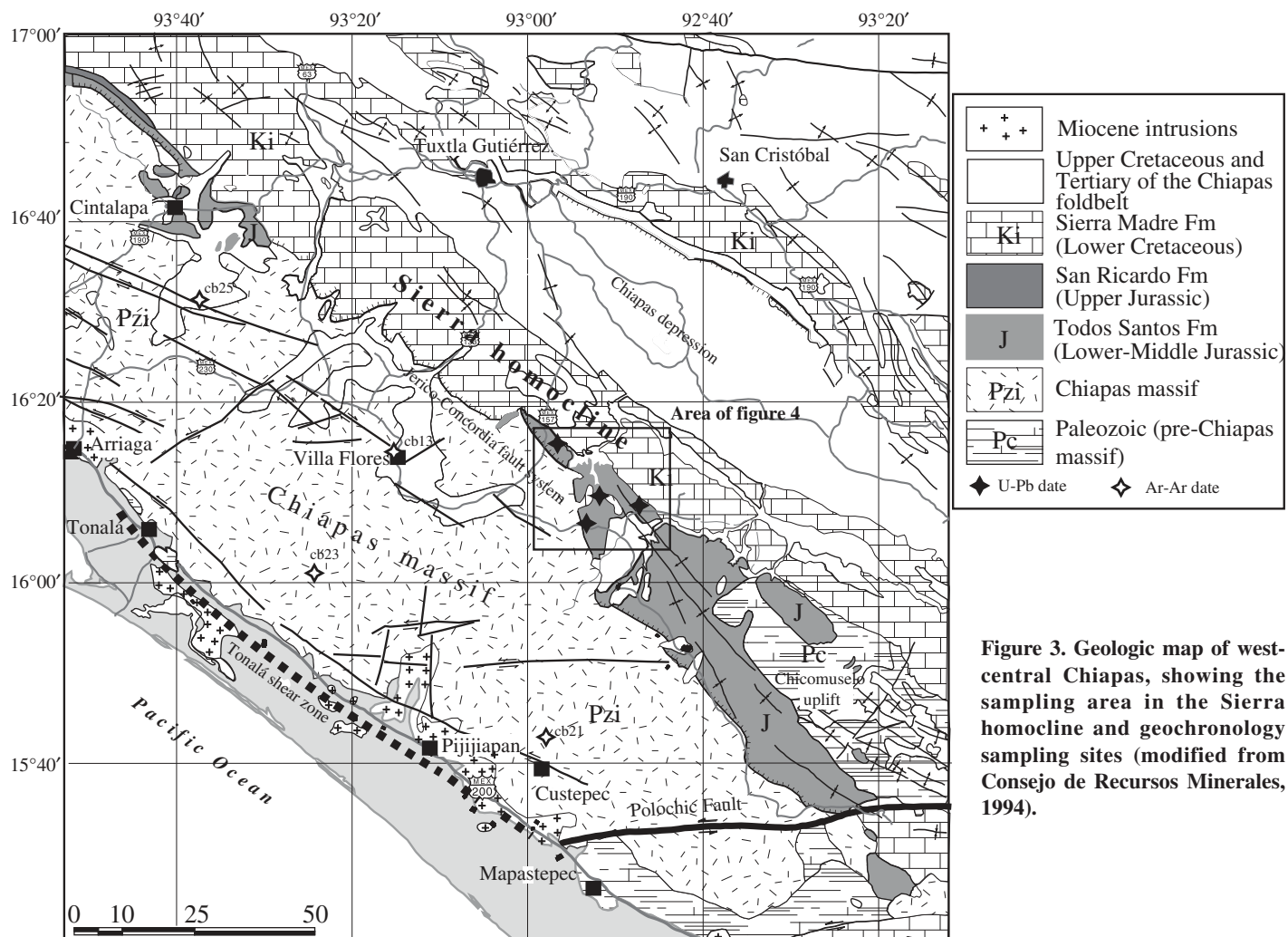


Figure 3. Geologic map of west-central Chiapas, showing the sampling area in the Sierra homocline and geochronology sampling sites (modified from Consejo de Recursos Minerales, 1994).

facies associations. The lowermost includes the arkosic sandstones described herein. A second association includes a conglomerate and coarse sandstone facies, which contains plane-parallel to massive stratification. Conglomerate clasts are commonly imbricated, and stratification is defined by 5 to 50-cm-thick discontinuous layers dominated by coarse-grained sandstone interbedded with layers dominated by pebbles and cobbles. The conglomerate facies is polymictic, but locally surrounded volcanic clasts constitute the dominant component. Other clasts include granitoids, slate, chert, and quartzite. Sandstone intervals are lithic (<70% quartz, >25% clasts, <5% feldspar), moderately to poorly sorted, poorly indurated, and subangular. Blair (1987) also recognized a facies association consisting of mudrock, silty sandstone, an uncommon lacustrine limestone facies with carbonaceous plant material, and rare tuffaceous horizons.

The upper part of the Jericó Member, which we refer to informally as the Concordia facies after outcrops west of the town of Concordia (Fig. 4), consists primarily of poorly sorted, hematitic, coarse-grained, conglomeratic sandstone in beds between 0.5 m and 2 m thick (Fig. 5E). Conglomerate clasts are well rounded and are dominated by metamorphic rocks, deep-seated plutonic rocks, and abundant quartz pebbles and cobbles. These red hematitic sandstones contain trough cross-beds, and are relatively well indurated. Siltstone and shale make up a small fraction of the succession. Toward the top of the section, rocks of the Jericó Member are commonly stained grayish-green by material derived from the overlying San Ricardo Formation. The contact with the San Ricardo Formation is transitional, marked by a gradual reduction in grain size and decrease in hematite cement.

The La Silla Formation was deposited upon and among large volcanic edifices, probably

stratovolcanoes, with a variety of fluvial and alluvial environments where volcanic material was reworked. The El Diamante Member is interpreted as a low-energy fluvial system on the basis of its abundant siltstone and claystone, deposited in overbank settings. The presence of mud drapes and mud chips suggests ephemeral streams. In the Jericó Member, in agreement with the interpretations of Blair (1987), we recognize alluvial fan environments in the conglomerate-sandstone facies association, lacustrine environments in the mudrock-limestone facies association, and a large-scale, high-energy, longitudinal fluvial environment in the arkosic sandstone facies. For the Concordia facies assemblage, amalgamated and discontinuous gravel and sandstone strata, with minor lenses of fine-grained material, suggest deposition in high-energy braided-fluvial systems that evolved with time into a lower energy coastal alluvial plain.

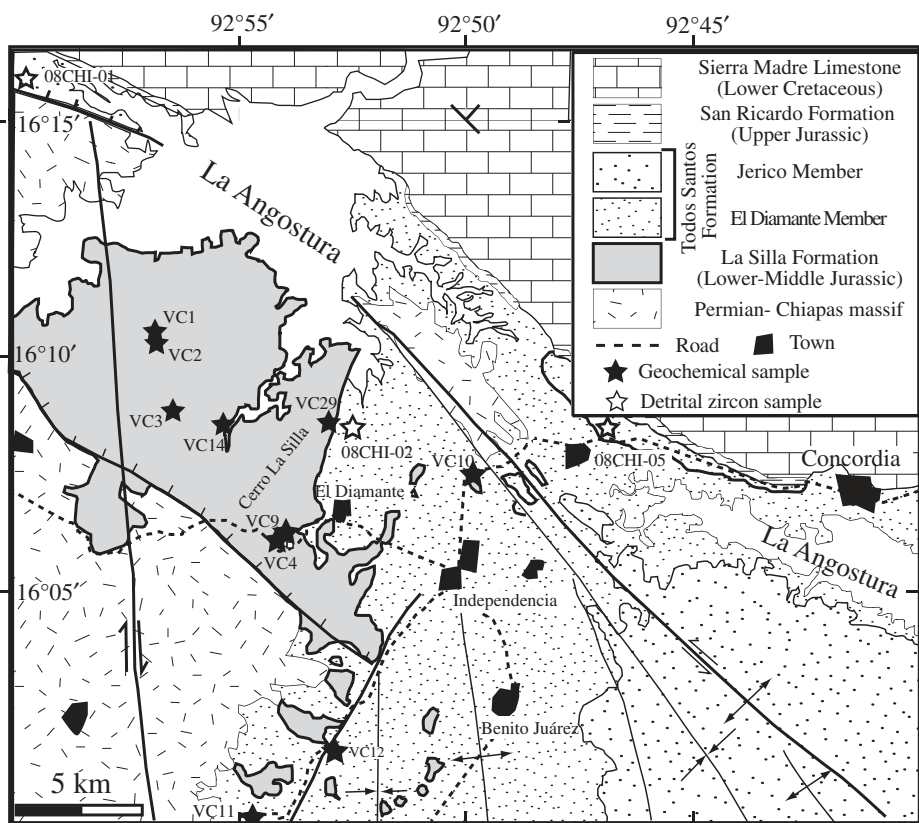


Figure 4. Geologic map of the Angostura lake area with sampling localities.

ANALYTICAL RESULTS

Detrital Zircon Geochronology

Detrital zircons were obtained from representative samples of the lower, middle, and upper part of the Todos Santos succession. One sample (08CHI-02) was collected near the base of the El Diamante Member, and two from the Jericó Member, one near the base (08CHI-01) and one high in the section (08CHI-05; Fig. 2). Jericó Member samples contain a large number of discordant grains (5% or greater), most of which were discarded as the analyses proceeded. The analyses, presented in stratigraphic order (Fig. 6), provide evidence for unroofing of the Chiapas massif, beginning with the Jurassic volcanic carapace, of which the La Silla Formation is part, followed by extensive denudation of the batholith complex. Zircons from the El Diamante Member show very little discordance, suggesting that Jurassic magmatism (described in the following) may have been responsible for discordance in older grains.

The sample from the El Diamante Member was collected from a sandstone channel, ~20 m above the contact with the underlying La Silla

Formation. The sample (08CHI-02) contains a nearly unimodal grain age population ranging from 196 to 161 Ma (Fig. 6), with a population peak near 178 Ma (Toarcian; n = 91). Of the grains analyzed, only one is Early-Middle Triassic, one is Late Permian, four are Grenville (ca. 1.1–1.0 Ga), and one is Paleoproterozoic (ca. 2.2 Ga). The dominant Jurassic grain population records erosion of Early to Middle Jurassic volcanic rocks from the Chiapas massif. This suggests that Jurassic rocks covered the massif prior to uplift. We regard the age range of the grains as a representative sample of the age range of volcanic activity in the region, with onset of magmatism in early Sinemurian time, near 196 Ma. The youngest grain age, ca. 161 Ma (Callovian-Oxfordian boundary), represented by a single grain, indicates the maximum depositional age of the El Diamante Member. Because an isolated zircon age may represent lead loss (e.g., Dickinson and Gehrels, 2009), a more conservative maximum depositional age of ca. 171 Ma is indicated by a cluster of 6 concordant grains with ages between ca. 172 and 169 Ma.

The lower part of the Jericó Member, despite its stratigraphic proximity to the granite contact, contains a diverse range of detrital zircon grain

ages. The sample (08CHI-01) was collected ~50 m above a nonconformable contact with a granitoid of the Chiapas batholith. The sample contains three dominant populations of grain ages: (1) Proterozoic grains ranging from 1639 to 977 Ma (peak near 1011 Ma; n = 26); (2) early Paleozoic grains ranging from 471 to 452 Ma (peak near 462 Ma; n = 13); and (3) a dominant Permian-Triassic population ranging from 281 to 208 Ma (peaks near 259, 245, and 210 Ma; n = 46). The youngest grains (ca. 210 Ma) appear to be part of a cluster of ages between ca. 190 and 210 with large analytical errors. Plotted on a concordia diagram they favor the existence of a source with an age of ca. 200 Ma, which has not been recognized in the Chiapas massif. Zircons derived from the Chiapas batholith dominate the sample, but it also contains many grains derived from early Paleozoic and Grenville basement, or grains recycled from upper Paleozoic rocks. The sample contains only three Jurassic grains, suggesting that Jurassic volcanic rocks had largely been eroded from the basement by onset of Jericó Member deposition.

The sample of the upper part of the Jericó Member, representing the Concordia facies, was collected ~200 m below the contact with the overlying San Ricardo Formation. The sample (08CHI-05) contains the most diverse suite of grain ages of the three samples (Fig. 6). There are five age populations present: (1) Paleo-proterozoic and Mesoproterozoic grains (ca. 1997–1450 Ma; n = 9); (2) a large population of Grenville grains (ca. 1251–904 Ma; n = 31); (3) Pan-African grains (ca. 719–556 Ma; n = 4); (4) early Paleozoic grains (~536–411 Ma; n = 14); (5) Permian and Triassic grains (ca. 287–201 Ma; n = 31, with a suggestion of a natural break between 236 and 208 Ma); and (6) Early Jurassic grains (ca. 199–175 Ma; n = 12). Analytical data are summarized in Table 1.

Geochemistry and Geochronology

We identify three different groups of volcanic rocks based on petrographic descriptions. These descriptions and microscope images are included in the Appendix.

Multielement diagrams for the volcanic rocks show enrichment in high ionic radius elements (Rb, Cs, Sr, Ba) with respect to high field strength elements (Fig. 7). There is enrichment in light rare earths (La, Ce, Eu) relative to heavy rare earths (Gd, Tb, Lu). In addition, there are positive anomalies of Ba, Pb, and Sr, and relative depletion of Nb and Ta. No geochemical data are available for the dikes.

Sample VC-4 (Fig. 4) is porphyritic, with phenocrysts consisting of ~75% plagioclase, 10% K-feldspar, 10% hornblende, and 5%

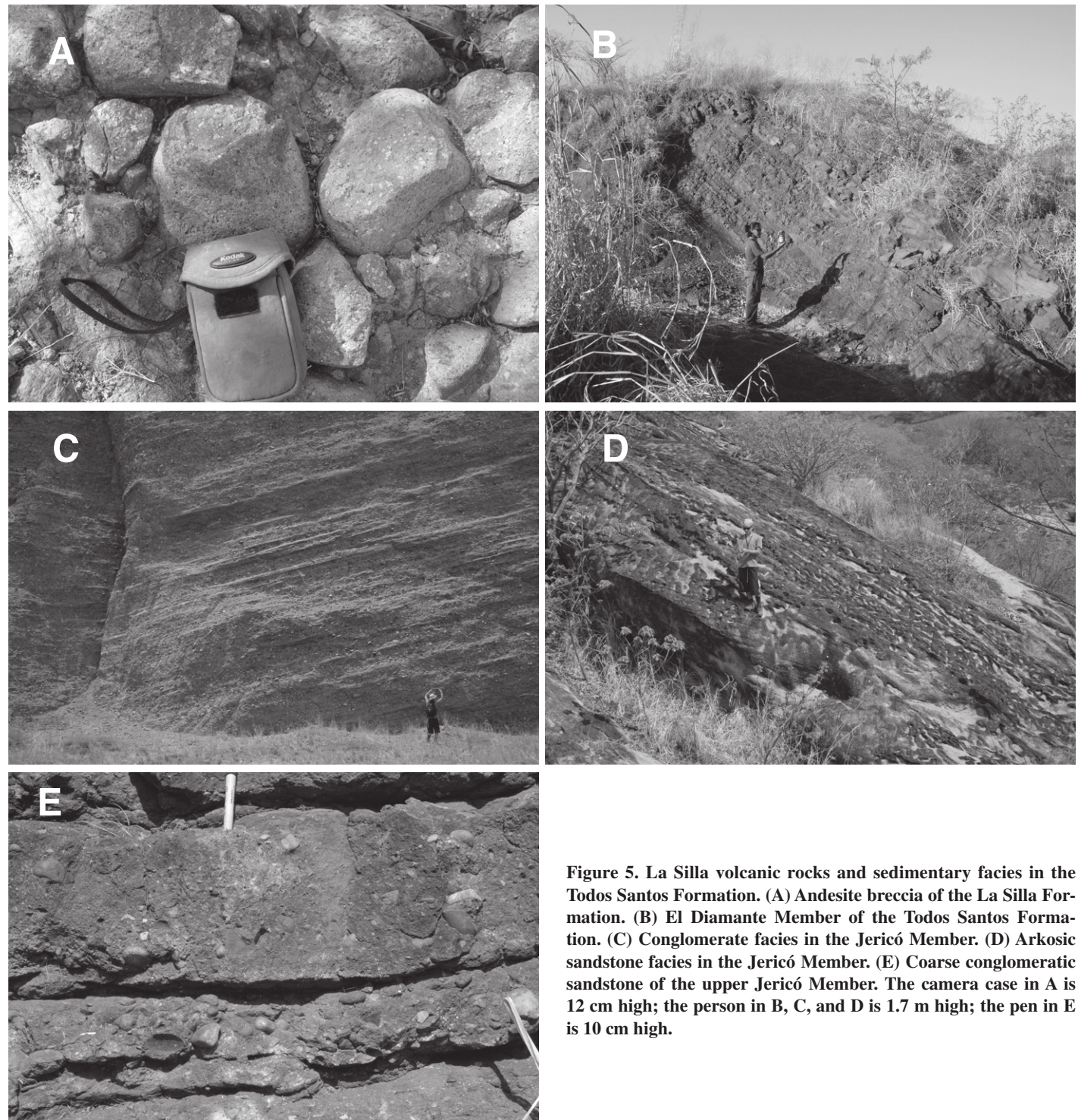


Figure 5. La Silla volcanic rocks and sedimentary facies in the Todos Santos Formation. (A) Andesite breccia of the La Silla Formation. (B) El Diamante Member of the Todos Santos Formation. (C) Conglomerate facies in the Jericó Member. (D) Arkosic sandstone facies in the Jericó Member. (E) Coarse conglomeratic sandstone of the upper Jericó Member. The camera case in A is 12 cm high; the person in B, C, and D is 1.7 m high; the pen in E is 10 cm high.

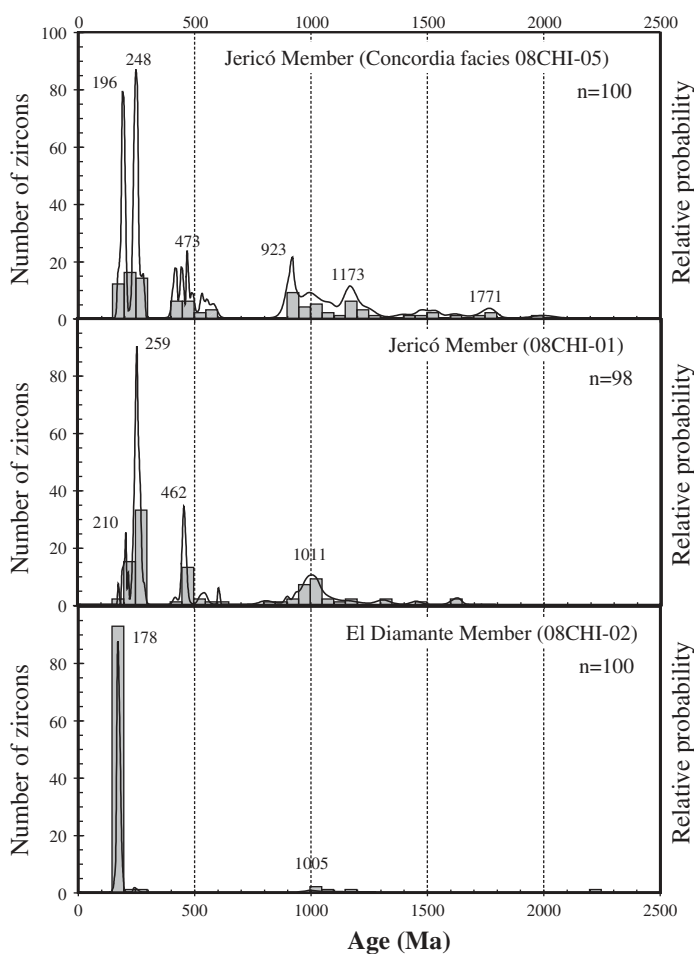


Figure 6. U-Pb age probability plots for detrital zircons of the Todos Santos Formation.

quartz. It is classified as an andesite. U-Th-Pb analyses were obtained from 12 grains selected by their morphology from cathodoluminescence images. The results are plotted on a Tera-Wasserburg diagram (Fig. 8). The great majority of the zircons analyzed are concordant, and the best estimate of the age of emplacement is 191.0 ± 3.0 Ma (Sinemurian–Pliensbachian; average of 11 grains). A single Late Permian zircon is interpreted as inherited, probably derived from partial melting of the Chiapas massif. Analytical data are summarized in Table 2.

Other evidence of Jurassic magmatism in the region is provided by numerous andesitic to basaltic dikes that intrude the Chiapas massif. We refer informally to this set of intrusions as the Cuscepec dike complex. The intrusions commonly occur in swarms of several parallel dikes. We present Ar-Ar analysis for these rocks in Figure 9. The Ar release spectra of the dikes have somewhat complex behavior; however, considering that generally the dikes do not have any minerals to separate, and that they show

very low-grade overprints, they provide useful constraints on the regional extent of magmatism. Analytical data are presented in Table 3, and summarized in Table 4. Typically, multiple experiments in the same rock sample yielded slightly climbing Ar release spectra, or saddle-shape spectra. The Ar release was not homogeneous. It is clear that the dikes are Jurassic in age, but the data do not allow precise age determinations. The best $^{40}\text{Ar}/^{39}\text{Ar}$ results, for sample CB25, are for hornblende separates from a porphyritic andesite, which could be of volcanic or hypabyssal origin. The inverse correlation age is 184.1 ± 3.4 Ma (mean square of weighted deviates, MSWD = 1.3).

INTERPRETATION

Detrital Zircon Provenance Data

The older Proterozoic grains in the Jericó Member have ca. 1620 Ma and 1456 Ma ages, which are largely absent from Mexican Gond-

wanan basement, and suggest an ultimate detrital source in Laurentian basement. However, it is likely that proximate sources of these grains were sedimentary or metasedimentary rocks of peri-Gondwanan basement that was near the depositional site of the Todos Santos Formation. Weber et al. (2008) found many zircons of such ages in pre-Ordovician metasedimentary basement of the southeastern Chiapas massif (Jocote unit) 50 km southeast of the study area, and also in para-amphibolites from the Cuscepec unit (Weber et al., 2007), and interpreted this as representing detrital sources from South America. It seems likely that 1.65 and 1.4 Ga zircons come from reworked metasediments of southeastern Chiapas or Guatemala. The Jocote unit is intruded by Ordovician (ca. 480 Ma) S-type granite (Weber et al., 2008). The early Paleozoic grains in Jericó sandstones are dominantly Ordovician, similar to ages in the Acatlán Complex of southern Mexico (Fig. 1), but they are more likely derived from local sources such as S-type granites in southeastern Chiapas or from the Altos Cuchumatanes (Solari et al., 2009). The clastic wedge derived from the Middle Ordovician Taconic orogen, a peri-Gondwanan collided arc of the southern Appalachians, contains an assemblage of grain ages near 1.7, 1.4, 0.9–1.1, and 0.5 Ga (Moecher and Samson, 2006), similar to that of our Concordia facies sample (08CHI-05). The southern Appalachians are along structural strike of the Gondwana-Laurentia suture from the pre-Gulf of Mexico position of the Maya block, so the similar age spectra are likely a result of analogous pre-Mesozoic basement ages in the peri-Gondwanan terrane collage. Permian–Triassic grains were derived directly from the basement of the Chiapas batholith, an inference supported by the arkosic composition of the Jericó Member.

It is possible that Proterozoic, Pan-African, Grenville, and older Proterozoic grains could have been derived from the upper Paleozoic Santa Rosa Formation, which has zircon populations of similar age (Weber et al., 2006); however, Santa Rosa strata are characterized by abundant Pan-African zircons and insignificant populations of Grenville grains. Grenville zircons in the Todos Santos Formation could be derived from Oaxacan basement (Keppie et al., 2003), Orinoquian basement (Restrepo-Pace et al., 1997), or, more likely, Maya block basement through erosion of metasedimentary host rocks of the Permian–Triassic Chiapas batholith (e.g., Weber et al., 2008).

Jurassic grains in the Todos Santos Formation were likely derived from nearby volcanic rocks. The age range of these grains, ca. 196–161 Ma, thus provides important

TABLE 1. U-Pb (ZIRCON) GEOCHRONOLOGIC ANALYSES OF TODOS SANTOS SANDSTONE SAMPLES IN CHIAPAS BY LASER ABLATION-MULTICOLLECTOR-INDUCTIVELY COUPLED PLASMA-MASS SPECTROMETRY

Analysis	U (ppm)	$^{206}\text{Pb}/^{204}\text{Pb}$	Isotope ratios			Apparent ages (Ma)			Conc. (%)				
			$^{207}\text{Pb}^*/^{235}\text{U}^*$	±	$^{207}\text{Pb}^*/^{235}\text{U}^*$	±	$^{206}\text{Pb}^*/^{238}\text{U}$	±					
08CH101-01 Todos Santos Formation, Jerico Member (UTM 15Q 501249 1799749)													
08CH101-66	57	1968	2.2	22.2412	10.4	0.1772	10.5	0.0286	1.5	0.14	181.7	2.6	-314.7
08CH101-6	65	2660	1.6	19.3702	8.6	0.2214	8.6	0.0311	1.0	0.11	197.4	1.9	73.4
08CH101-43	843	11728	0.7	19.8830	3.6	0.2201	3.9	0.0317	1.6	0.40	201.4	3.1	96.5
08CH101-55	397	15196	1.5	19.6725	2.7	0.2301	4.7	0.0328	1.0	0.40	208.2	9.6	89.3
08CH101-91	255	11088	1.9	20.5526	5.4	0.2206	6.2	0.0329	3.2	0.51	208.6	6.6	158.9
08CH101-85	468	6388	2.6	17.1801	12.1	0.2656	12.1	0.0331	0.8	0.07	209.9	1.7	39.0
08CH101-40	607	23040	2.1	20.0823	1.7	0.2279	2.2	0.0332	1.4	0.65	210.5	3.0	113.5
08CH101-15	958	28396	3.2	19.7885	3.1	0.2318	3.7	0.0333	2.0	0.54	211.0	4.2	96.1
08CH101-72	29	1224	1.4	27.9794	32.0	0.1736	32.0	0.0352	1.0	0.03	223.1	2.2	-34.3
08CH101-27	353	14572	8.7	19.8667	2.5	0.2604	3.1	0.0375	1.7	0.56	237.5	4.0	112.8
08CH101-29	117	5168	1.6	19.9074	3.6	0.2666	4.0	0.0385	1.8	0.44	243.5	4.2	118.3
08CH101-7	458	23316	1.5	19.9117	3.8	0.2703	3.9	0.0390	3.1	0.63	246.9	7.6	120.3
08CH101-12	159	7168	1.7	19.4705	10.3	0.2770	10.4	0.0391	1.6	0.16	247.4	7.6	96.3
08CH101-31	213	9776	1.5	20.0021	2.9	0.2714	3.3	0.0394	1.5	0.47	248.9	3.8	127.8
08CH101-89	376	21192	2.5	19.4840	1.8	0.2786	2.9	0.0394	2.2	0.77	248.9	5.4	97.5
08CH101-82	295	13160	1.8	19.6017	2.8	0.2770	3.5	0.0394	2.1	0.59	248.3	7.6	103.4
08CH101-62	42	2144	2.3	22.3339	14.6	0.2437	14.8	0.0395	2.2	0.15	249.5	5.3	-367.6
08CH101-14	77	3304	1.5	18.3817	11.9	0.3003	11.9	0.0400	1.0	0.08	253.1	2.4	65.3
08CH101-57	56	3168	1.9	19.7025	10.1	0.2803	10.4	0.0401	2.4	0.23	253.2	5.8	110.2
08CH101-58	390	19908	2.0	19.7220	2.2	0.2808	2.2	0.0402	1.2	0.46	251.3	2.9	111.6
08CH101-28	155	7320	1.4	20.3038	4.1	0.2743	4.3	0.0404	1.3	0.30	255.3	3.3	160.3
08CH101-78	142	8372	1.4	19.9808	5.3	0.2791	7.0	0.0404	4.6	0.65	255.6	11.5	129.6
08CH101-80	295	15404	1.5	19.2859	2.9	0.2895	4.0	0.0405	2.8	0.69	255.9	6.9	91.8
08CH101-44	146	7052	1.2	19.9606	4.3	0.2798	4.4	0.0405	0.9	0.20	256.0	2.2	128.3
08CH101-97	172	8352	1.5	20.1453	4.3	0.2790	4.4	0.0408	0.7	0.16	257.6	1.7	144.6
08CH101-37	115	4752	1.0	19.7692	8.0	0.2858	8.0	0.0410	0.5	0.07	258.9	1.4	116.7
08CH101-81	427	22128	3.9	19.6396	1.3	0.2877	3.3	0.0410	3.0	0.91	258.9	7.5	109.2
08CH101-68	74	4536	1.1	20.5995	12.1	0.2745	12.3	0.0410	2.4	0.19	259.1	6.0	205.8
08CH101-18	183	8644	1.5	19.6478	2.6	0.2896	3.5	0.0416	2.1	0.79	260.7	6.1	110.4
08CH101-3	246	6664	1.2	16.4505	16.2	0.3462	16.4	0.0413	2.1	0.13	260.9	5.2	41.3
08CH101-45	550	27904	8.1	19.3087	0.8	0.2950	3.0	0.0413	2.9	0.97	261.0	7.5	94.5
08CH101-13	361	15772	1.6	19.3954	2.0	0.2937	2.9	0.0413	2.1	0.71	261.0	5.3	98.2
08CH101-75	320	16240	5.9	19.2879	1.6	0.2965	3.2	0.0415	3.2	0.89	263.6	8.2	94.0
08CH101-18	268	13096	1.5	19.5821	1.7	0.2927	2.7	0.0416	2.1	0.79	262.0	8.2	107.7
08CH101-100	141	9028	5.2	20.1189	5.5	0.2855	5.9	0.0417	2.2	0.37	263.1	13.3	145.2
08CH101-99	239	11016	1.7	19.7155	2.4	0.2918	4.4	0.0417	3.7	0.83	263.5	9.4	115.5
08CH101-9	135	6984	1.5	19.5038	6.1	0.2952	6.5	0.0418	2.2	0.34	263.7	5.7	104.2
08CH101-26	239	12136	2.7	19.5918	3.7	0.2941	4.6	0.0418	2.9	0.61	263.9	7.4	108.8
08CH101-49	170	9028	3.0	19.6353	3.7	0.2954	3.7	0.0421	0.8	0.22	265.7	2.1	111.8
08CH101-42	229	10164	1.9	19.1392	4.8	0.3038	5.2	0.0422	2.1	0.40	266.2	5.4	89.6
08CH101-87	98	5444	2.2	19.9347	5.3	0.2989	3.1	0.0423	2.4	0.78	266.9	6.2	105.2
08CH101-22	440	24292	6.9	19.4993	1.9	0.2989	1.9	0.0423	1.1	0.34	271.1	7.6	277.0
08CH101-96	244	7696	1.1	19.0453	3.0	0.3109	3.1	0.0429	1.1	0.34	271.9	5.0	139.3
08CH101-1	135	7384	1.6	19.9976	4.7	0.2970	5.1	0.0431	1.9	0.37	271.9	5.0	-813.4
08CH101-35	47	2504	2.6	22.0198	12.9	0.2698	12.9	0.0431	1.0	0.08	272.0	2.7	13.3
08CH101-94	127	1652	1.7	13.1837	19.3	0.4562	19.9	0.0436	4.9	0.25	275.4	63.3	25.3
08CH101-79	98	5444	2.2	18.1664	1.9	0.5156	2.9	0.0679	2.3	0.77	276.7	14.3	136.6
08CH101-22	440	15444	1.6	19.4206	2.9	0.3117	3.0	0.0439	0.5	0.18	277.0	1.5	105.4
08CH101-21	221	7384	2.7	19.5846	1.5	0.3110	1.8	0.0442	1.0	0.53	278.7	2.6	278.7
08CH101-24	226	12076	1.9	19.5856	1.7	0.3135	3.9	0.0445	3.5	0.90	280.8	9.7	115.4
08CH101-74	171	8972	3.2	19.6116	2.6	0.3246	3.1	0.0462	1.7	0.56	280.4	4.9	121.0
08CH101-48	153	11020	0.9	18.1664	1.9	0.5156	2.9	0.0679	2.3	0.77	282.2	10.2	102.3
08CH101-8	464	45760	4.0	17.7505	1.4	0.5650	2.1	0.0727	1.6	0.76	452.6	7.0	97.2
08CH101-33	282	24720	5.7	18.1699	2.0	0.5540	2.1	0.0730	0.7	0.33	454.2	3.1	109.8

(continued)

TABLE 1. U-Pb (ZIRCON) GEOCHRONOLOGIC ANALYSES OF TODOS SANTOS SANDSTONE SAMPLES IN CHIAPAS BY LASER ABLATION-MULTICOLLECTOR-INDUCTIVELY COUPLED PLASMA-MASS SPECTROMETRY (*continued*)

Analysis	U (ppm)	Isotope ratios						Apparent ages (Ma)											
		$^{206}\text{Pb}/^{204}\text{Pb}$	$^{206}\text{Pb}^*/^{207}\text{Pb}^*$	\pm	$^{207}\text{Pb}^*/^{235}\text{U}^*$	\pm	$^{206}\text{Pb}^*/^{238}\text{U}$	\pm	Error correction	$^{206}\text{Pb}^*/^{238}\text{U}$	\pm	$^{206}\text{Pb}^*/^{235}\text{U}$	\pm	$^{206}\text{Pb}^*/^{207}\text{Pb}^*$	\pm	Best age (Ma)	\pm	Conc. (%)	
88CHI-01 Todos Santos Formation, Jerico Member (UTM 15Q 501249 1799749) (continued)																			
95 88CHI01-69	7860	2.5	18.1246	3.4	0.5959	3.8	0.0735	1.7	0.44	457.5	7.4	451.2	13.8	419.2	7.56	457.5	7.4	109.1	
510 88CHI01-38	29456	3.2	17.5139	1.9	0.5814	2.5	0.0738	1.7	0.67	459.3	7.4	465.3	9.3	495.3	40.8	459.3	7.4	92.7	
1078 88CHI01-14	66704	4.4	17.7626	1.1	0.5740	2.5	0.0739	2.2	0.89	459.9	9.7	460.6	9.1	464.1	24.8	459.9	9.7	99.1	
219 88CHI01-67	18156	1.8	17.6815	1.6	0.5790	1.7	0.0742	0.6	0.34	461.7	2.6	463.8	6.4	474.3	35.7	461.7	2.6	97.4	
12240 88CHI01-70	133	3.1	17.9509	2.4	0.5713	2.6	0.0744	1.1	0.44	462.4	5.1	458.8	9.6	440.7	52.3	462.4	5.1	104.9	
74 88CHI01-36	6884	1.3	18.2473	3.9	0.5635	4.2	0.0746	1.3	0.32	463.6	15.2	453.8	15.2	404.2	88.2	463.6	6.0	114.7	
140 88CHI01-90	13940	10.3	18.0371	2.0	0.5703	2.9	0.0746	2.1	0.72	463.8	9.5	458.2	10.8	430.0	45.4	463.8	9.5	107.9	
219 88CHI01-30	20456	1.7	18.0036	1.7	0.5733	2.5	0.0749	1.9	0.74	465.3	8.4	460.1	9.3	434.2	37.5	465.3	8.4	107.2	
72 88CHI01-53	6716	1.1	18.1567	3.5	0.5728	3.7	0.0754	1.2	0.32	468.8	5.2	459.8	13.6	415.3	78.0	468.8	5.2	112.9	
35 88CHI01-34	29032	2.2	17.6557	2.0	0.5911	2.4	0.0757	1.3	0.56	470.3	6.1	471.6	9.0	477.5	43.9	470.3	6.1	98.5	
523 88CHI01-77	45268	5.5	17.5712	1.1	0.5948	3.0	0.0758	2.8	0.93	471.0	12.5	473.9	11.2	488.1	23.9	471.0	12.5	96.5	
242 88CHI01-90	23852	2.2	17.2566	1.6	0.6890	2.6	0.0862	2.1	0.78	533.2	10.5	532.2	10.9	527.8	36.0	533.2	10.5	101.0	
182 88CHI01-84	20916	2.3	17.1486	1.1	0.7106	3.7	0.0884	3.6	0.96	545.9	18.7	545.1	15.7	541.5	23.1	545.9	18.7	100.8	
180 88CHI01-41	18072	1.8	17.2234	1.5	0.7173	2.3	0.0896	1.8	0.77	553.2	9.6	532.0	9.9	532.2	32.3	532.2	9.6	104.0	
251 88CHI01-46	17980	1.3	16.3359	1.5	0.8383	1.7	0.0993	0.6	0.38	610.4	3.7	618.2	7.7	646.8	32.9	610.4	3.7	94.4	
289 88CHI01-88	59384	5.6	14.3698	1.7	1.2844	3.5	0.1339	3.1	0.88	809.8	23.8	838.8	20.2	916.3	34.0	809.8	23.8	88.4	
149 88CHI01-16	26224	2.6	13.9953	2.9	1.4009	7.2	0.1422	6.6	0.91	857.0	52.8	889.3	42.7	970.4	59.6	857.0	52.8	88.3	
127 88CHI01-65	22200	3.3	14.0633	1.9	1.4755	2.2	0.1505	1.2	0.52	903.8	9.8	920.4	13.5	960.5	39.1	903.8	9.8	94.1	
52 88CHI01-64	9744	4.8	14.3602	2.1	1.5074	2.4	0.1570	1.2	0.50	940.0	10.7	933.4	14.8	917.7	43.3	940.0	10.7	102.4	
127 88CHI01-51	24544	3.0	13.9523	1.6	1.6427	1.7	0.1662	0.7	0.40	991.3	6.2	986.8	10.7	976.6	31.6	976.6	31.6	101.1	
201 88CHI01-51	36536	2.3	13.9514	1.2	1.6397	1.7	0.1659	1.2	0.70	989.6	11.1	985.6	10.8	976.8	24.9	976.8	24.9	101.3	
196 88CHI01-52	44044	8.7	13.8783	1.2	1.6176	3.2	0.1628	3.0	0.93	972.4	26.9	977.0	20.2	987.5	24.4	987.5	24.4	98.5	
654 88CHI01-59	117636	3.7	13.8595	0.9	1.6643	3.6	0.1673	3.5	0.97	997.2	32.5	995.0	23.1	990.2	18.9	990.2	18.9	100.7	
54 88CHI01-63	12320	2.7	13.8559	1.8	1.6892	2.2	0.1697	1.4	0.62	1010.7	13.0	1004.5	14.3	990.9	35.9	990.9	35.9	102.0	
140 88CHI01-5	26544	2.9	13.8538	1.4	1.6732	3.2	0.1681	2.9	0.90	1001.7	26.4	998.4	20.2	991.1	28.5	991.1	28.5	101.1	
59 88CHI01-9	9244	1.9	13.8111	2.1	1.7113	2.7	0.1714	1.7	0.64	1019.9	16.3	1012.8	17.4	997.3	42.4	997.3	42.4	102.3	
195 88CHI01-52	45640	7.5	13.7808	1.1	1.6711	1.7	0.1670	1.2	0.74	995.7	11.4	997.6	10.7	1001.8	22.9	1001.8	22.9	99.4	
98 88CHI01-83	27224	4.4	13.7574	1.5	1.7026	2.5	0.1689	2.0	0.81	1011.4	19.1	1009.5	16.7	1005.3	30.5	1005.3	30.5	100.6	
121 88CHI01-54	27308	2.6	13.7068	1.7	1.7318	2.7	0.1722	2.1	0.78	1024.0	19.7	1020.4	17.1	1012.7	33.7	1012.7	33.7	101.1	
103 88CHI01-47	20544	3.2	13.6649	2.1	1.7471	2.7	0.1732	1.8	0.66	1029.4	17.1	1026.1	17.7	1018.9	41.7	1018.9	41.7	101.0	
354 88CHI01-60	63964	2.7	13.6564	1.6	1.6602	3.4	0.1644	3.0	0.88	981.4	27.6	993.5	21.8	1020.2	33.0	1020.2	33.0	96.2	
102 88CHI01-76	24796	3.9	13.6286	1.1	1.7386	3.3	0.1719	3.2	0.95	1022.3	29.8	1023.0	21.5	1024.3	21.9	1024.3	21.9	99.8	
433 88CHI01-93	96584	4.7	13.6141	0.7	1.7073	1.9	0.1886	1.8	0.93	1004.2	16.9	1011.3	12.5	1026.5	14.2	1026.5	14.2	97.8	
182 88CHI01-93	38292	2.8	13.5380	1.2	1.7751	1.7	0.1743	1.2	0.70	1035.7	11.5	1036.4	11.1	1037.8	24.7	1037.8	24.7	99.8	
230 88CHI01-61	55504	2.9	13.5145	2.7	1.7694	3.5	0.1734	2.3	0.64	1031.0	21.5	1034.3	22.8	1041.3	54.3	1041.3	54.3	99.0	
187 88CHI01-56	40724	2.7	13.4217	2.2	1.7099	4.3	0.1665	3.7	0.86	992.5	34.3	1012.3	27.8	1055.2	44.5	1055.2	44.5	94.1	
361 88CHI01-86	51748	2.0	13.2232	1.5	1.7786	1.7	0.1706	0.7	0.44	1015.3	7.0	1037.7	10.8	1085.1	29.9	1085.1	29.9	93.6	
208 88CHI01-50	45152	2.8	13.1049	2.8	1.9581	5.9	0.1842	5.2	0.88	1089.9	52.1	1094.3	39.5	1103.1	55.4	1103.1	55.4	98.8	
302 88CHI01-2	63716	5.2	12.6874	2.9	1.9169	3.6	0.1764	2.1	0.59	1047.2	20.5	1087.0	33.9	1167.6	57.3	1167.6	57.3	89.7	
184 88CHI01-17	1844	3.3	12.6379	2.0	1.9015	5.2	0.1847	4.8	0.93	1092.8	48.4	1098.4	35.4	1175.3	39.0	1175.3	39.0	93.0	
257 88CHI01-71	60260	3.0	11.7862	1.8	1.5785	2.9	0.2204	2.3	0.79	1284.1	27.0	1294.6	21.4	1312.0	34.7	1312.0	34.7	97.9	
253 88CHI01-32	65200	3.2	11.7558	1.3	2.6278	3.1	0.2240	2.8	0.90	1303.2	32.4	1308.4	22.5	1317.0	26.0	1317.0	26.0	99.0	
312 88CHI01-23	33540	2.6	10.9358	1.1	3.1942	1.2	0.2633	0.5	0.42	1455.7	6.5	1455.8	9.2	1455.8	20.6	1455.8	20.6	100.0	
319 94384	1.6	10.0429	1.0	3.8752	2.6	0.2823	2.4	0.93	1602.7	34.6	1608.5	21.2	1616.1	17.9	1616.1	17.9	99.2		
291 109028	3.1	9.9210	0.8	3.9696	3.6	0.2856	3.5	0.98	1619.7	49.7	1628.0	28.8	1638.8	14.3	1638.8	14.3	98.8		
177 88CHI02-28	3332	1.3	16.8237	11.5	0.0253	2.0	0.17	161.1	3.2	191.3	20.4	250.5	161.1	250.5	161.1	250.5	161.1	27.6	
97 88CHI02-76	14496	1.1	22.5374	17.0	0.1624	17.2	0.0265	2.9	0.17	168.9	4.8	152.8	40.8	419.3	4.8	419.3	4.8	98.8	
86 88CHI02-16	1680	1.5	15.7661	10.9	0.2344	11.2	0.0268	2.3	0.21	170.5	3.9	213.8	21.5	722.6	170.5	722.6	170.5	23.6	
157 88CHI02-30	7544	1.1	19.5815	4.7	0.1892	5.8	0.0269	3.4	0.58	171.0	5.7	176.0	9.3	243.9	107.9	243.9	107.9	70.1	
69 88CHI02-6	3524	1.6	19.6030	14.4	0.1897	14.9	0.0270	3.5	0.24	171.6	5.9	176.4	24.1	241.4	334.3	241.4	334.3	71.1	
122 9376	1.3	19.2647	11.3	0.1939	11.7	0.0271	3.2	0.27	172.3	5.4	172.3	19.3	281.4	172.3	281.4	172.3	27.6		

IRANIAN

TABLE 1. U-Pb (ZIRCON) GEOCHRONOLOGIC ANALYSES OF TODOS SANTOS SANDSTONE SAMPLES IN CHIAPAS BY LASER ABLATION-MULTICOLLECTOR-INDUCTIVELY COUPLED PLASMA-MASS SPECTROMETRY (continued)

Analysis	U (ppm)	$^{206}\text{Pb}/^{204}\text{Pb}$	Isotope ratios			Apparent ages (Ma)			Conc. (%)					
			$^{207}\text{Pb}^*/^{206}\text{Pb}^*$	\pm	$^{207}\text{Pb}^*/^{235}\text{U}^*$ (%)	$^{206}\text{Pb}^*/^{238}\text{U}$ (%)	\pm	Error correction		$^{206}\text{Pb}^*/^{207}\text{Pb}^*$ (Ma)	\pm	Best age (Ma)	\pm	
08CHI02 Todos Santos Formation, El Diamante Member (UTM 15Q 513192 1784462) (continued)														
08CHI02-91	129	7262	1.7	18.7921	8.0	0.1989	9.1	0.0271	4.4	0.48	172.4	7.4	181.9	172.4
08CHI02-33	71	5644	1.2	21.4720	12.9	0.1747	13.3	0.0272	3.0	0.23	173.1	5.1	173.1	173.1
08CHI02-8	14948	0.7	20.1748	4.5	0.1862	4.8	0.0272	1.6	0.34	173.3	2.8	173.3	173.3	
08CHI02-24	517	6164	1.6	22.3091	13.7	0.1686	13.8	0.0273	1.2	0.08	173.5	2.0	166.2	99.2
08CHI02-20	164	3088	1.1	16.33464	7.7	0.2305	7.9	0.0273	1.8	0.23	173.8	3.1	173.8	173.8
08CHI02-95	96	708	0.9	15.3378	20.8	0.2469	20.9	0.0275	2.4	0.12	174.7	4.2	174.7	174.7
08CHI02-86	1542	62448	1.0	20.0679	1.0	0.1888	1.6	0.0275	1.2	0.76	174.8	2.5	184.2	184.2
08CHI02-29	218	10368	1.1	21.0045	5.3	0.1805	6.1	0.0275	2.9	0.49	174.9	5.1	174.9	174.9
08CHI02-4	141	4084	1.5	19.8426	7.0	0.1911	7.4	0.0275	2.3	0.32	174.9	4.0	177.6	177.6
08CHI02-20	163	12228	1.5	20.3511	3.7	0.1864	3.8	0.0275	1.0	0.25	175.0	1.7	173.6	173.6
08CHI02-3	174	7132	0.9	20.6784	7.0	0.1840	7.1	0.0276	1.2	0.17	175.5	2.1	171.5	171.5
08CHI02-15	90	5892	2.2	21.7204	13.2	0.1753	13.2	0.0276	1.3	0.10	175.6	2.2	164.0	20.1
08CHI02-93	85	3604	1.0	17.4290	5.8	0.2185	6.2	0.0276	2.1	0.35	175.7	3.7	200.7	11.2
08CHI02-74	151	13368	1.4	20.5382	7.9	0.1855	8.1	0.0276	1.8	0.22	175.7	3.1	172.8	12.9
08CHI02-78	149	9396	0.8	20.6237	9.7	0.1847	9.8	0.0276	1.3	0.13	175.7	2.2	172.1	15.5
08CHI02-9	49	4144	1.7	24.0096	17.1	0.1589	17.4	0.0277	3.1	0.18	175.9	5.4	149.7	24.3
08CHI02-10	89	5124	1.5	20.3535	9.5	0.1875	9.7	0.0277	1.9	0.20	176.0	3.3	174.5	15.6
08CHI02-20	259	7660	1.4	19.3220	7.2	0.1977	7.3	0.0277	1.2	0.17	176.2	2.1	183.2	12.2
08CHI02-17	137	10136	1.5	21.4523	7.0	0.1783	7.2	0.0277	2.0	0.27	176.4	3.4	166.6	11.1
08CHI02-64	117	5696	1.1	18.5380	16.1	0.2065	16.3	0.0278	2.7	0.16	176.5	4.6	190.6	28.4
08CHI02-61	87	7288	1.1	21.3599	15.0	0.1792	15.1	0.0278	2.3	0.15	176.5	3.9	167.4	23.4
08CHI02-50	44	4596	1.4	20.8539	18.7	0.1838	19.2	0.0278	4.5	0.23	176.8	7.8	171.3	30.3
08CHI02-18	89	4048	1.1	21.4000	13.3	0.1791	13.3	0.0278	1.0	0.08	176.8	1.8	167.3	20.6
08CHI02-31	150	16148	1.2	20.9242	5.0	0.1832	5.1	0.0278	1.4	0.26	176.8	2.4	165.2	12.2
08CHI02-87	64	3736	1.2	18.6312	7.4	0.2058	7.5	0.0278	1.2	0.16	176.8	2.1	166.6	11.1
08CHI02-85	126	6932	1.5	19.5186	8.0	0.1965	8.1	0.0278	1.4	0.18	176.9	2.5	182.1	13.6
08CHI02-98	192	2180	0.8	15.1733	21.4	0.2531	21.5	0.0279	2.1	0.10	177.1	3.7	229.1	44.1
08CHI02-79	87	2552	1.4	16.0606	10.3	0.2396	10.8	0.0279	3.1	0.29	177.4	5.4	174.1	44.1
08CHI02-82	84	5668	0.9	21.6191	11.7	0.1782	12.2	0.0279	3.3	0.27	177.7	5.8	166.6	18.7
08CHI02-75	50	3412	0.7	20.6031	16.2	0.1871	16.3	0.0280	2.1	0.13	177.7	3.7	174.1	26.1
08CHI02-57	101	7264	1.4	20.9761	9.5	0.1838	10.0	0.0280	3.1	0.31	177.8	5.4	171.4	15.7
08CHI02-26	175	6412	0.9	19.9321	4.8	0.1936	5.1	0.0280	1.7	0.33	177.9	2.9	179.7	8.3
08CHI02-51	73	2928	1.1	14.1443	45.9	0.2733	46.3	0.0280	5.8	0.13	178.3	1.4	167.4	245.3
08CHI02-83	216	26848	1.3	20.3058	2.8	0.1906	4.1	0.0281	3.0	0.73	178.5	5.3	177.7	16.6
08CHI02-70	123	10512	1.1	19.9781	7.0	0.1939	7.2	0.0281	1.9	0.27	178.7	3.4	180.0	11.9
08CHI02-65	117	11288	1.8	20.3444	6.0	0.1909	6.2	0.0282	1.3	0.21	179.0	2.2	177.4	10.1
08CHI02-41	94	3112	1.2	19.0379	5.7	0.2043	6.1	0.0282	2.1	0.34	179.4	3.7	188.8	10.5
08CHI02-27	75	5800	1.6	21.7144	9.7	0.1792	9.8	0.0282	0.8	0.08	179.4	7.7	167.4	10.5
08CHI02-94	164	5528	2.1	21.1154	11.4	0.1844	11.7	0.0282	2.5	0.21	179.5	4.4	171.8	18.5
08CHI02-73	107	11976	1.3	19.7814	9.3	0.1968	9.7	0.0282	2.5	0.26	179.5	4.5	182.4	16.1
08CHI02-89	129	24540	1.5	21.0180	7.8	0.1856	8.1	0.0283	2.1	0.26	179.8	3.8	172.9	12.9
08CHI02-2	135	7280	1.4	19.5548	6.7	0.2000	7.6	0.0284	3.7	0.48	180.3	6.5	185.1	12.9
08CHI02-49	99	9188	1.6	20.7428	3.4	0.1886	4.8	0.0284	3.4	0.70	180.4	6.0	175.5	7.7
08CHI02-25	280	18152	1.1	20.3238	3.5	0.1933	4.8	0.0285	3.3	0.69	181.1	5.9	179.4	7.9
08CHI02-19	64	5528	1.4	19.4843	8.8	0.2010	9.3	0.0284	2.7	0.29	180.5	4.9	185.9	15.7
08CHI02-62	146	10532	1.4	19.9923	10.4	0.1959	10.5	0.0284	1.5	0.14	180.6	2.6	181.6	17.5
08CHI02-47	130	7692	1.2	21.1885	9.1	0.1851	9.7	0.0284	1.7	0.18	180.8	3.0	172.4	14.4
08CHI02-67	52	5180	1.3	16.7642	12.3	0.2340	12.5	0.0285	2.5	0.20	180.9	4.4	213.5	24.1
08CHI02-49	280	18152	1.1	20.3238	3.5	0.1933	4.8	0.0285	3.3	0.69	181.1	5.9	179.4	7.9
08CHI02-91	110	7716	1.5	21.8131	8.2	0.1801	8.9	0.0285	3.4	0.39	181.1	6.1	168.2	13.7
08CHI02-72	132	10072	1.2	21.1390	6.0	0.1862	6.0	0.0285	0.9	0.15	181.4	1.6	173.4	16.4
08CHI02-11	117	5804	1.2	20.5982	11.0	0.1917	11.2	0.0286	1.9	0.17	182.0	3.3	178.1	18.3
08CHI02-100	956	13260	0.2	20.2542	1.3	0.1950	3.3	0.0286	3.0	0.92	182.1	5.4	165.5	29.8
08CHI02-96	129	1260	1.4	12.9095	8.1	0.3061	8.3	0.0287	1.9	0.23	182.2	3.5	113.3	16.1

(continued)

TABLE 1. U-Pb (ZIRCON) GECHRONOLOGIC ANALYSES OF TODOS SANTOS SANDSTONE SAMPLES IN CHIAPAS BY LASER ABLATION-MULTICOLLECTOR-INDUCTIVELY COUPLED PLASMA-MASS SPECTROMETRY (*continued*)

Analysis	U (ppm)	Isotope ratios			Apparent ages (Ma)			Conc. (%)		
		$^{206}\text{Pb}/^{204}\text{Pb}$	$^{206}\text{Pb}^*/^{207}\text{Pb}^*$	\pm (%)	$^{206}\text{Pb}^*/^{238}\text{U}$	\pm (%)	Error correction		$^{206}\text{Pb}^*/^{235}\text{U}$	\pm (Ma)
88CHI-02 Todos Santos Formation, El Diamante Member (UTM 15Q 513192 1784462) (continued)										
88CHI02-79a	104	2964	1.4	15.9549	22.7	0.0287	3.9	0.17	182.4	7.1
88CHI02-60	89	16848	1.7	21.1510	8.6	0.1872	8.8	0.24	182.5	46.5
88CHI02-99	253	13716	1.1	20.6958	3.6	0.1914	3.9	0.287	174.2	14.1
88CHI02-56	79	2504	1.2	14.8743	12.9	0.2663	13.3	0.287	177.8	6.3
88CHI02-69	70	4884	1.5	20.1659	15.0	0.0287	2.4	0.24	182.6	2.4
88CHI02-14	163	11228	0.9	20.9725	5.4	0.1965	1.6	0.29	175.8	6.3
88CHI02-52	93	6704	1.6	21.6353	12.0	0.1832	12.3	0.0287	184.9	85.1
88CHI02-23	130	7712	1.2	21.2397	7.8	0.1868	8.0	0.288	173.9	3.5
88CHI02-36	115	8060	0.7	20.1496	7.1	0.1974	7.3	0.0288	182.9	12.8
88CHI02-5	78	22094	1.3	22.2094	13.0	0.1791	2.2	0.17	183.3	2.7
88CHI02-80	57	5624	1.2	22.8883	20.4	0.0289	2.1	0.10	183.5	4.0
88CHI02-39	217	12016	1.1	20.4605	3.1	0.1946	3.6	0.0289	162.8	3.8
88CHI02-63	70	4920	1.3	21.3180	18.5	0.1870	19.3	0.0289	182.7	9.1
88CHI02-77	85	5696	1.4	19.4365	12.4	0.2058	12.5	0.0290	173.9	53.3
88CHI02-58	150	8920	1.4	20.0801	5.0	0.1995	6.5	0.0291	182.9	24.9
88CHI02-59	57	6124	1.7	21.8132	10.7	0.1839	11.0	0.0291	182.7	4.0
88CHI02-48	88	10168	1.5	21.8710	16.3	0.1837	16.5	0.0291	175.7	9.0
88CHI02-71	69	5472	1.4	20.9219	6.8	0.1924	6.8	0.0292	182.7	4.0
88CHI02-42	69	1376	1.3	13.3596	14.1	0.3016	15.3	0.0292	182.7	4.0
88CHI02-84	299	13492	1.0	19.6960	3.8	0.2046	5.1	0.0292	182.7	4.0
88CHI02-81	95	10552	1.0	20.6556	12.3	0.1954	12.3	0.0293	182.7	4.0
88CHI02-37	52	2924	1.4	18.7173	12.7	0.2159	12.7	0.0293	182.7	4.0
88CHI02-53	126	7232	1.4	18.8889	4.3	0.2143	6.9	0.0295	182.7	4.0
88CHI02-44	316	17596	1.4	19.7821	3.0	0.2066	3.0	0.0296	182.7	4.0
88CHI02-97	211	7056	1.1	19.0439	2.9	0.2147	3.5	0.0297	182.7	4.0
88CHI02-38	585	19088	0.7	20.1491	2.6	0.2039	2.9	0.0298	182.7	4.0
88CHI02-55	133	14440	1.2	18.7189	9.6	0.2198	9.8	0.0298	182.7	4.0
88CHI02-66	120	8360	1.6	20.6424	6.8	0.1996	7.7	0.0299	182.7	4.0
88CHI02-54	54	6276	1.3	24.2197	19.8	0.1708	19.9	0.0300	182.7	4.0
88CHI02-35	50	4936	1.3	23.2877	15.4	0.1783	15.7	0.0301	182.7	4.0
88CHI02-34	122	15248	1.8	20.5403	9.9	0.2027	10.0	0.0302	182.7	4.0
88CHI02-40	197	10416	1.3	20.3469	4.8	0.2051	4.9	0.0303	182.7	4.0
88CHI02-45	134	13860	1.4	20.1243	5.4	0.2085	5.7	0.0304	182.7	4.0
88CHI02-43	77	6412	1.4	18.3922	5.5	0.2318	5.9	0.0309	182.7	4.0
88CHI02-21	265	24508	1.0	19.9141	4.5	0.2721	5.0	0.0393	182.7	4.0
88CHI02-32	261	10088	1.7	18.7436	5.1	0.3018	5.9	0.0410	182.7	4.0
88CHI02-46	144	35472	2.8	13.7735	1.4	0.6231	2.5	0.1621	182.7	4.0
88CHI02-12	573	153048	8.0	13.7692	1.0	1.6421	2.8	0.1640	182.7	4.0
88CHI02-13	400	181536	12.8	13.2673	1.9	1.8815	3.1	0.1810	182.7	4.0
88CHI02-7	125	9536	2.5	12.5863	3.8	1.9901	4.4	0.1817	182.7	4.0
88CHI02-88	145	584	1.3	7.1950	12.3	0.6137	12.4	0.0320	182.7	4.0
88CHI-05 Todos Santos Formation, Jerico Member-Concordia Facies (UTM 15Q 523389 1784138)										
88CHI05-54	98	3464	1.0	21.5902	8.1	0.1762	8.4	0.0276	182.7	3.2
88CHI05-3	159	4624	0.7	20.1837	6.1	0.1934	6.6	0.0283	182.7	3.2
88CHI05-45	137	5356	1.5	20.9332	10.6	0.1904	10.6	0.0289	182.7	3.2
88CHI05-57	440	13992	1.7	19.9046	2.3	0.2026	2.8	0.0293	182.7	3.2
88CHI05-14	109	5492	1.6	20.9025	6.4	0.1990	6.6	0.0302	182.7	3.2
88CHI05-87	84	1560	1.5	16.4184	18.4	0.2535	18.8	0.0302	182.7	3.2
88CHI05-33	77	1660	0.7	15.5082	15.5	0.2725	15.6	0.0306	182.7	3.2
88CHI05-78	157	6716	2.1	20.2895	3.5	0.2096	3.7	0.0308	182.7	3.2
88CHI05-95	368	13620	1.1	20.1870	2.1	0.2107	2.6	0.0308	182.7	3.2
88CHI05-70	68	3856	2.3	23.3557	17.6	0.1924	17.7	0.0309	182.7	3.2

(continued)

TABLE 1. U-Pb (ZIRCON) GEOCHRONOLOGIC ANALYSES OF TODOS SANTOS SANDSTONE SAMPLES IN CHIAPAS BY LASER ABLATION-MULTICOLLECTOR-INDUCTIVELY COUPLED PLASMA-MASS SPECTROMETRY (continued)

Analysis	U (ppm)	206Pb/ 204Pb	Isotope ratios			Apparent ages (Ma)			Conc. (%)						
			207Pb*/ 205Pb*	±	235U* (%)	206Pb*/ 238U* (%)	±	Error correction		206Pb*/ 235U (Ma)	±	206Pb*/ 207Pb* (Ma)	±	Best age (Ma)	±
08CHI05 Todos Santos Formation, Jerico Member-Concordia Facies (UTM15Q 523389 1784138) (continued)															
08CHI05-77	151	6380	1.2	20.7616	5.7	0.2068	6.3	0.0311	2.6	0.42	197.7	5.1	190.9	11.0	107.4
08CHI05-80	221	6504	0.6	17.9482	13.9	0.2405	14.1	0.0313	2.1	0.15	198.7	4.1	218.9	27.7	135.7
08CHI05-35	140	4671	1.7	18.8068	10.4	0.2327	1.3	0.0317	1.3	0.12	201.4	2.5	212.4	20.2	310.7
08CHI05-64	154	5616	1.5	19.8885	6.6	0.2204	6.8	0.0318	1.4	0.21	201.8	2.8	202.2	12.4	237.2
08CHI05-84	145	5504	1.4	20.2502	6.1	0.2177	6.7	0.0320	2.7	0.40	202.9	5.4	200.0	12.2	153.8
08CHI05-63	323	12552	1.3	19.7515	2.3	0.2255	4.5	0.0323	3.9	0.86	204.9	7.8	206.5	8.4	143.8
08CHI05-30	427	15588	3.3	19.4209	1.5	0.2330	2.9	0.0328	2.5	0.86	208.1	5.1	212.6	5.5	224.0
08CHI05-1	115	5008	2.1	20.7141	6.7	0.2186	6.9	0.0328	1.8	0.26	208.3	3.6	200.7	12.6	112.8
08CHI05-2	122	4884	0.9	20.8335	5.1	0.2176	5.6	0.0329	2.2	0.39	208.5	4.5	200.5	10.2	99.2
08CHI05-82	44	2548	2.1	20.8699	21.2	0.2464	21.5	0.0373	3.6	0.17	236.0	8.3	223.6	43.2	507.0
08CHI05-53	272	13764	2.3	19.2388	4.6	0.2726	5.0	0.0380	2.0	0.39	240.6	4.7	244.8	10.9	236.0
08CHI05-38	300	16604	1.4	19.7505	3.9	0.2682	4.1	0.0384	1.2	0.29	243.0	2.8	241.2	8.8	224.0
08CHI05-22	320	15796	1.6	19.5573	2.7	0.2718	3.7	0.0386	2.5	0.69	243.8	6.0	244.1	8.0	246.8
08CHI05-55	247	47360	1.8	19.9840	3.6	0.2671	4.1	0.0387	1.8	0.45	244.8	4.4	240.4	8.7	196.8
08CHI05-40	83	5272	1.2	20.1426	9.6	0.2688	9.7	0.0393	1.0	0.10	248.3	2.4	241.7	20.8	178.4
08CHI05-9	151	9776	1.7	19.3849	3.6	0.2794	3.6	0.0393	1.7	0.42	248.4	4.1	250.2	8.9	224.5
08CHI05-79	417	19124	1.1	19.7503	2.7	0.2752	3.4	0.0394	2.0	0.61	249.2	5.0	246.8	7.4	224.0
08CHI05-36	289	16072	2.2	19.7109	5.7	0.2763	6.7	0.0395	3.5	0.52	249.7	5.0	247.8	14.7	228.7
08CHI05-61	281	13632	2.4	20.1677	4.8	0.2711	5.2	0.0397	2.1	0.40	250.7	5.1	243.6	11.2	175.5
08CHI05-28	361	18744	2.5	19.4524	2.5	0.2826	4.5	0.0399	3.8	0.84	252.0	9.5	252.7	10.2	299.7
08CHI05-62	122	5704	1.5	19.8904	3.7	0.2775	3.7	0.0400	0.5	0.13	253.0	1.2	248.7	8.2	207.7
08CHI05-60	153	6052	1.5	19.1383	5.4	0.2895	5.6	0.0402	1.3	0.24	254.0	3.3	258.2	12.7	266.4
08CHI05-32	249	15300	2.3	19.9731	3.2	0.2832	3.3	0.0410	0.9	0.26	259.2	2.2	253.2	7.4	249.2
08CHI05-59	116	5864	1.6	20.3269	7.8	0.2784	7.9	0.0410	1.2	0.15	259.3	3.1	249.4	17.5	243.8
08CHI05-76	125	4956	1.7	17.3851	13.3	0.3276	13.5	0.0413	2.6	0.19	261.0	6.5	243.6	31.1	287.8
08CHI05-46	44	2612	2.0	21.8379	13.0	0.2609	13.0	0.0413	0.6	0.05	261.1	1.6	235.4	27.3	314.6
08CHI05-11	47	3100	2.1	22.4758	15.3	0.2539	15.5	0.0414	2.1	0.14	261.4	5.4	229.7	31.8	-53.4
08CHI05-29	141	8812	3.3	19.9080	5.6	0.2868	5.8	0.0414	1.5	0.26	261.6	3.9	256.0	22.7	253.0
08CHI05-34	532	29304	2.1	18.9286	10.1	0.3034	10.6	0.0436	3.4	0.32	263.0	8.8	269.0	31.1	249.4
08CHI05-76	62	3516	1.7	21.4950	11.7	0.2794	11.8	0.0436	1.7	0.14	274.9	4.6	250.2	26.2	280.9
08CHI05-67	188	10812	1.4	19.4690	4.2	0.3159	4.7	0.0446	2.0	0.44	281.3	5.6	278.7	11.4	257.2
08CHI05-7	217	12144	1.8	19.2572	3.1	0.3268	3.3	0.0456	1.2	0.35	287.7	3.3	287.1	8.3	282.3
08CHI05-29	483	45108	2.3	18.0173	2.8	0.5040	3.0	0.0559	1.4	0.46	411.2	5.7	414.4	10.7	325.5
08CHI05-85	462	45684	8.9	17.6773	1.6	0.5253	1.9	0.0673	1.0	0.53	420.2	4.2	428.7	6.8	474.8
08CHI05-69	151	16028	2.2	18.4303	2.5	0.5062	4.7	0.0677	4.0	0.84	422.1	16.1	415.9	16.0	381.8
08CHI05-48	279	13844	1.9	17.9343	3.0	0.5256	3.1	0.0684	0.9	0.28	426.3	3.6	428.9	10.9	442.8
08CHI05-7	352	38432	1.4	17.7572	3.7	0.5548	4.6	0.0715	2.7	0.58	427.1	3.5	476.6	14.9	471.5
08CHI05-26	381	31508	3.1	18.0264	2.2	0.5404	2.5	0.0720	1.1	0.46	448.1	11.4	448.2	16.5	464.8
08CHI05-65	338	37244	13.5	17.7974	2.0	0.5486	2.5	0.0731	1.7	0.30	454.8	7.4	468.3	12.8	475.7
08CHI05-23	106	8792	2.2	17.2018	5.4	0.5859	5.7	0.0731	1.6	0.69	455.1	10.9	458.5	16.1	475.7
08CHI05-98	402	35216	1.9	17.6700	2.4	0.5707	3.5	0.0731	2.5	0.72	467.9	10.3	442.1	10.3	422.1
08CHI05-72	151	13840	0.9	17.9395	2.7	0.5853	2.7	0.0762	0.5	0.18	473.1	2.3	467.9	10.3	426.3
08CHI05-56	136	15808	2.2	17.7037	3.8	0.5909	3.9	0.0769	0.8	0.20	477.7	3.5	476.6	9.3	485.0
08CHI05-19	131	17536	1.7	16.7529	1.7	0.7753	3.3	0.0788	2.2	0.75	488.9	10.5	483.8	11.4	477.7
08CHI05-81	118	17592	3.0	16.8667	2.0	0.7798	3.2	0.0954	2.5	0.79	587.4	14.2	585.4	14.3	577.7
08CHI05-86	343	25236	4.2	17.4270	1.7	0.6323	2.3	0.0799	1.6	0.69	495.7	7.7	497.5	9.2	466.2
08CHI05-44	393	48956	2.2	17.1030	2.4	0.6853	4.6	0.0850	3.9	0.84	525.9	19.4	530.0	12.8	525.9
08CHI05-68	310	39664	2.9	17.2974	2.1	0.6917	2.5	0.0868	1.2	0.50	536.4	6.3	533.8	10.2	522.6
08CHI05-73	285	32016	0.5	17.0491	1.4	0.7290	2.2	0.0901	1.6	0.74	556.4	8.6	556.0	9.3	556.4
08CHI05-81	131	17536	1.7	16.7529	1.7	0.7753	3.3	0.0942	3.3	0.89	580.3	18.1	582.8	16.2	592.4
08CHI05-10	118	20204	2.7	13.7275	3.7	1.5127	4.4	0.1506	2.4	0.55	904.4	20.2	923.5	12.2	909.4
08CHI05-39	74	34440	4.6	14.3164	1.4	1.4592	2.0	0.1515	1.5	0.72	909.4	12.5	928.8	12.2	909.4
08CHI05-21	150	32100	2.2	14.4829	1.0	1.4580	2.8	0.1531	2.6	0.93	918.6	22.2	913.2	16.7	900.1
08CHI05-25	128	13320	2.9	14.3211	3.7	1.4786	4.7	0.1536	3.0	0.64	921.0	25.9	921.6	28.7	923.3

(continued)

TABLE 1. U-Pb (ZIRCON) GEOCHRONOLOGIC ANALYSES OF TODOS SANTOS SANDSTONE SAMPLES IN CHIAPAS BY LASER ABLATION-MULTICOLLECTOR-INDUCTIVELY COUPLED PLASMA-MASS SPECTROMETRY (continued)

Analysis	U (ppm)	Isotope ratios						Apparent ages (Ma)									
		$^{206}\text{Pb}/^{204}\text{Pb}$	$^{207}\text{Pb}^*/^{204}\text{Pb}^*$	\pm	$^{206}\text{Pb}^*/^{235}\text{U}^*$	\pm	$^{206}\text{Pb}^*/^{238}\text{U}^*$	\pm	Error correction	$^{206}\text{Pb}^*/^{235}\text{U}$	\pm	$^{207}\text{Pb}^*/^{206}\text{Pb}^*$	\pm	Best age (Ma)	\pm	Conc. (%)	
08CHI05 Todos Santos Formation, Jerico Member-Concordia Facies (UTM 15Q 5233889 1784138) (continued)																	
08CHI05-49	77	17352	1.8	14.5269	2.7	1.4619	5.3	0.1540	4.5	0.86	923.5	38.8	914.8	31.7	923.5	38.8	103.3
08CHI05-41	116	25912	2.4	14.2239	2.3	1.4937	2.4	0.1541	0.7	0.28	923.9	5.9	927.8	14.7	923.9	5.9	98.6
08CHI05-91	161	46132	3.3	14.4636	1.5	1.4699	2.2	0.1542	1.7	0.74	924.4	14.4	918.1	13.6	924.4	14.4	102.4
08CHI05-89	87	21880	3.5	14.3907	1.5	1.4806	2.6	0.1545	2.2	0.82	926.3	18.6	922.5	15.8	926.3	18.6	101.4
08CHI05-58	515	91496	2.4	14.0221	1.3	1.5269	4.7	0.1553	4.5	0.96	930.5	39.0	941.2	28.7	966.5	39.0	96.3
08CHI05-94	76	16948	0.7	14.0453	1.6	1.5656	4.3	0.1595	4.0	0.93	953.9	35.2	956.7	26.4	963.1	31.8	953.9
08CHI05-100	348	80252	2.8	13.8880	1.2	1.6607	1.7	0.1673	1.1	0.68	997.1	10.4	993.7	10.6	986.0	25.0	101.1
08CHI05-74	140	31148	3.1	13.8109	1.5	1.7218	2.9	0.1725	2.5	0.86	1025.7	23.4	1016.7	18.5	987.4	30.1	102.8
08CHI05-93	125	261188	2.9	13.7950	2.4	1.6888	2.7	0.1690	1.2	0.44	1006.4	10.9	1004.3	16.9	999.7	48.4	100.7
08CHI05-13	326	72636	3.0	13.7811	1.7	1.7004	3.7	0.1700	3.3	0.88	1011.9	30.6	1008.7	23.7	1001.8	35.1	101.0
08CHI05-97	239	51152	2.8	13.7732	1.2	1.6884	2.7	0.1687	2.5	0.90	1004.7	22.8	1004.1	17.5	1002.9	24.8	100.2
08CHI05-71	310	38088	2.5	13.5836	2.6	1.7184	3.2	0.1693	1.9	0.59	1008.2	17.7	1004.1	20.8	1031.0	53.0	97.8
08CHI05-15	278	63708	2.7	13.5367	1.3	1.8004	2.5	0.1768	2.1	0.84	1049.2	20.2	1015.4	16.2	1038.0	26.9	101.1
08CHI05-31	287	51088	5.7	13.4787	1.7	1.6934	2.6	0.1655	1.9	0.76	987.5	17.8	1006.1	16.3	1046.7	33.5	94.3
08CHI05-92	186	46456	4.3	13.3256	1.2	1.7410	2.5	0.1683	2.2	0.87	1002.5	20.0	1023.8	15.9	1089.7	24.5	93.7
08CHI05-96	273	57568	4.6	13.1683	0.9	1.9229	2.0	0.1836	1.8	0.89	1086.9	18.2	1089.1	13.6	1093.5	18.4	99.4
08CHI05-52	228	68144	3.9	12.8059	1.1	2.0200	1.6	0.1876	1.1	0.71	1108.4	11.5	1122.3	10.8	1149.1	22.1	96.5
08CHI05-50	216	54488	2.4	12.7654	2.0	2.0871	4.2	0.1932	3.6	0.87	1138.8	37.9	1144.6	28.6	1155.4	40.5	98.6
08CHI05-37	323	82752	3.1	12.7351	1.5	2.1470	3.0	0.1983	2.6	0.87	1166.2	27.7	1164.1	20.7	1160.1	29.0	100.5
08CHI05-99	168	47960	2.0	12.6844	0.9	2.1618	1.3	0.1989	1.0	0.75	1169.3	10.5	1168.8	9.1	1168.0	17.2	100.1
08CHI05-66	354	65920	4.0	12.6589	1.5	2.1421	4.7	0.1967	4.5	0.95	1157.4	47.4	1162.5	32.7	1172.0	30.3	98.8
08CHI05-90	160	44216	5.3	12.5864	1.1	2.1769	1.9	0.1987	1.5	0.81	1168.4	16.0	1173.7	12.9	1183.4	21.6	98.7
08CHI05-24	185	49928	3.3	12.5512	1.0	2.1998	2.8	0.2002	2.6	0.93	1176.7	28.2	1181.0	19.6	1188.9	19.8	99.0
08CHI05-37	100	27996	2.3	12.4009	3.0	2.2265	3.2	0.2003	1.2	0.37	1176.7	12.8	1189.4	22.4	1212.7	58.3	97.0
08CHI05-42	111	14860	2.8	12.2988	4.1	2.1808	4.2	0.1944	0.6	0.15	1145.4	6.7	1174.9	29.1	1229.7	81.0	93.1
08CHI05-16	311	64344	3.5	12.2690	1.7	2.4280	3.1	0.2161	2.6	0.84	1261.0	29.3	1250.9	22.0	1233.7	32.8	102.2
08CHI05-18	262	77060	2.1	12.1617	1.6	2.4401	2.6	0.2152	2.0	0.79	1256.6	23.3	1254.5	18.5	1250.9	30.7	100.5
08CHI05-51	161	45400	2.2	11.2369	1.7	2.7981	2.0	0.2280	1.1	0.55	1324.2	13.2	1355.0	15.1	1404.0	32.4	94.3
08CHI05-4	87	24424	2.0	10.8212	1.2	3.2506	1.8	0.2551	1.4	0.76	1464.8	17.8	1469.3	13.9	1475.8	22.2	99.3
08CHI05-43	678	40596	2.3	10.6575	1.5	2.8166	1.6	0.2177	0.6	0.39	1269.8	7.3	1360.0	12.1	1504.7	28.0	84.4
08CHI05-20	169	54812	1.8	10.4441	1.1	3.3954	2.8	0.2572	2.6	0.92	1475.5	33.6	1503.3	21.8	1542.8	21.1	95.6
08CHI05-6	46	20600	1.7	10.0242	1.6	3.9281	3.3	0.2856	2.9	0.87	1619.4	41.5	1619.5	26.9	1619.6	30.0	100.0
08CHI05-83	147	25328	1.6	9.4538	2.9	3.6675	2.9	0.2515	0.5	0.17	1446.0	6.5	1564.3	23.1	1727.8	52.4	83.7
08CHI05-75	174	68124	1.3	9.2950	1.4	4.6763	2.7	0.3152	2.2	0.84	1766.5	34.6	1763.0	22.2	1758.9	26.2	100.4
08CHI05-27	381	36976	1.3	9.1699	1.3	4.2039	2.1	0.2796	1.6	0.78	1589.3	22.7	1674.8	17.0	1753.6	23.9	89.1
08CHI05-5	119	47204	1.2	8.1317	2.6	6.1490	2.8	0.3626	1.2	0.43	1994.7	20.8	1997.2	24.8	1999.8	45.7	99.7

Notes: All uncertainties are reported at the 1-sigma level, and include only measurement errors. Systematic errors would increase age uncertainties by 1%–2%. Common Pb correction is from ^{204}Pb , with composition interpreted from Stacey and Kramers (1975) and uncertainties of 1.0 for $^{206}\text{Pb}/^{204}\text{Pb}$, 0.3 for $^{207}\text{Pb}/^{204}\text{Pb}$, $^{208}\text{Pb}/^{204}\text{Pb}$ fractionation is calibrated relative to fragments of a large Sri Lanka zircon of 564 ± 4 Ma (2-sigma). U decay constants and composition as follows: $^{238}\text{U} = 9.8485 \times 10^{-10}$, $^{235}\text{U} = 1.55125 \times 10^{-10}$, $^{232}\text{Th} = 1.37388$. “Best age” column indicates interpreted age of grain by inspection of data, generally using ca. 1.1 Ga as the cross-over value for $^{206}\text{Pb}/^{238}\text{U}$ and $^{207}\text{Pb}/^{206}\text{Pb}$ ages. “Conc.” is percent concordance (= $^{206}\text{Pb}/^{238}\text{U}$ age/ $^{207}\text{Pb}/^{206}\text{Pb}$ age $\times 100$). Sample location Universal Transverse Mercator (UTM) datum utilize NAD27 MEXICO.

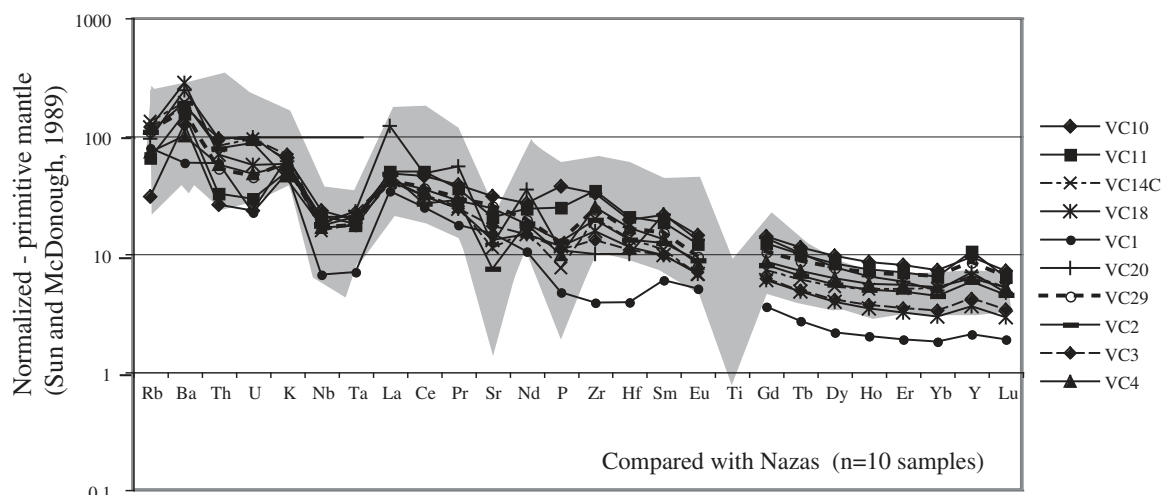


Figure 7. Normalized multielement spider diagrams for samples collected from six different outcrops of pre-Oxfordian volcanic rocks in the La Silla and Todos Santos Formations (for sample location, see Fig. 4). Sample elemental abundances are normalized to the primitive mantle values of Sun and McDonough (1989). The gray fields for comparison correspond to data for the Nazas arc of Barboza-Gudiño et al. (2008).

insight into the age range of Jurassic magmatism in Chiapas and vicinity. The age span of these grains encompasses the age of the subjacent La Silla Formation (described in the following section). Moreover, we do not observe post-170 Ma grain ages upsection through the Todos Santos Formation, indicating that volcanic activity had ceased, or nearly ceased, after initial (or during) deposition of the Todos Santos Formation.

Geochemistry and Geochronology of Jurassic Magmatism

The volcanic assemblage has characteristics of typical arc melts. The rocks from the La Silla Formation (Fig. 7) are compared with contemporaneous Jurassic arc volcanism from the central (Mexican Altiplano) and eastern (Sierra Madre Occidental) outcrop belts of the Nazas Formation after Barboza-Gudiño et al. (2008); their samples are generally more differentiated. This explains why negative Sr anomalies, for example, are more pronounced. The positive anomalies of Ba, Pb, and Sr, and relative depletion of Nb and Ta are considered a geochemical characteristic of magmatic arcs (Hawkesworth et al., 1993). The volcanic rocks have weak alteration due to weathering and burial, but Nb and Ta anomalies relative to other relatively immobile rare earths such as Th and La suggest that this is a reliable indicator of subduction-related magmas.

The range of ages for four dikes analyzed is 184–150 Ma (Table 5); this is in relatively good

agreement with the range of detrital zircon age data and with a single U-Pb SHRIMP-RG age determination. There are younger ages in the dikes, but these ages are for samples yielding high MSWD values in inverse correlation diagrams (Fig. 9). The ca. 150–160 Ma ages suggest that there was Late Jurassic magmatism, but a more conservative approach is to consider these as minimum ages related to cooling and/or Ar loss by very low grade metamorphism. We have, however, observed mafic dikes that intruded Todos Santos strata near Motozintla along the Mexico-Guatemala border outside of our field area. Despite the low precision of the results, it is apparent that the dikes correspond closely to the volcanic episode correlative with the La Silla Formation as defined by detrital zircon data. The $^{40}\text{Ar}/^{39}\text{Ar}$ data also demonstrate that Jurassic magmatism was widespread in the Chiapas massif and its eastern margin, from Uzpanapa to Custepec (Fig. 1).

DISCUSSION

U-Pb zircon geochronology for volcanic rocks of the La Silla Formation corroborates previous lower precision K-Ar age determinations indicating Jurassic volcanism in Chiapas, but appears to restrict magmatism to pre-early-Late Jurassic time. The 191 ± 3 Ma U-Pb age indicates that arc magmatism was under way in the region in Sinemurian–Pliensbachian time, and detrital zircon U-Pb ages from the El Diamante Member of the Todos Santos Formation indicate that magmatism began as early as

196 Ma (early Sinemurian). The $^{40}\text{Ar}/^{39}\text{Ar}$ geochronology suggests that magmatism extended into the early part of the Late Jurassic, which is younger than the Sinemurian–latest Callovian age range (ca. 196–161 Ma) of detrital zircons in the Todos Santos Formation; however, the $^{40}\text{Ar}/^{39}\text{Ar}$ ages are interpreted as minimum ages and some of the dikes may be related to rift magmatism. The geochronology and geochemistry indicate that pre-Oxfordian continental arc magmatism occurred on the western region of the Maya block.

The geochronology also suggests that the rift deposits represented by axial-fluvial deposits of the Jericó facies and associated alluvial fan deposits are Oxfordian or younger. The close relationship of the rift deposits with the Jericó-Concordia fault system (Fig. 3; Blair, 1987; Movarec, 1983) suggests that rifting initiated in an area originally occupied by arc volcanism. The detrital zircon provenance data are consistent with rapid erosional removal of the Jurassic volcanic carapace and denudation of the Chiapas massif, with dominant sources in the Permian complex for the lower Jericó and deep-seated Grenville, Ordovician, and other metasedimentary sources for the upper Jericó Member.

An Early–Middle Jurassic (pre-Oxfordian, ca. 200–160 Ma) continental volcanic arc is represented by the Nazas Formation of the Mexican Altiplano and northeastern Mexico (Fig. 10; Pantoja-Alor, 1963; Blickwede, 1981; Jones et al., 1995; Barboza-Gudiño et al., 1998, 2004, 2008). The Nazas Formation is a volcanic

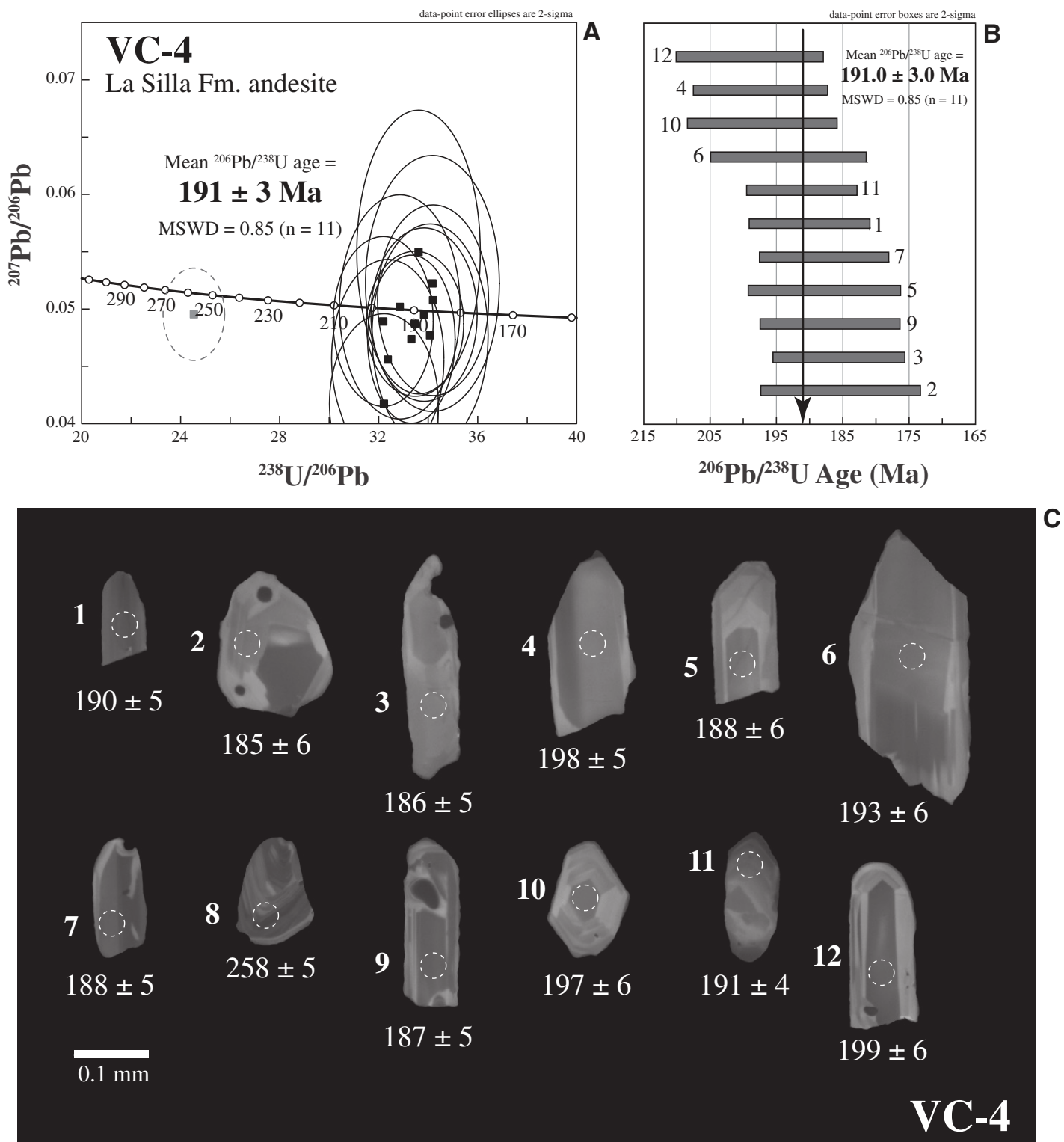


Figure 8. (A) Tera-Wasserburg diagram for U-Pb isotope ratios of zircons for sample VC-4 (Fig. 4). Error ellipses of individual spots are 2σ . (B, C) Zircons used for age calculation (ages in Ma). MSWD—mean square of weighted deviations.

TABLE 2. TRACE ELEMENT GEOCHEMISTRY FOR VOLCANIC SAMPLES OF LA SILLA AND TODOS SANTOS FORMATIONS

Sample	VC-10 Basalt	VC-11 Basalt	VC-13 Dacite	VC-14C Dacite	VC-18 Dacite	VC-1 Rhyodacite	VC-20 Dacite	VC-29 Dacite	VC-2 Dacite	VC-3 Andesite	VC-4 Andesite
Li	29.1	14.8	1.3	25.3	37.2	29.2	26.3	31.5	34.7	39.7	37.1
Be	1.99	2.12	2.57	1.46	1.50	1.09	1.33	1.52	1.67	1.81	1.85
P (wt%) P ₂ O ₅	0.82	0.54	0.02	0.17	0.25	0.10	0.23	0.27	0.28	0.24	0.21
Sc	23.2	22.5	3.0	8.7	8.8	5.3	11.6	16.8	10.0	8.5	10.4
V	83	76	6	46	53	40	66	133	99	75	62
Cr	159.8	84.1	3.4	7.8	8.7	4.0	16.1	26.1	14.1	13.5	8.9
Co	25.0	20.0	1.0	5.9	6.7	6.7	15.4	13.5	9.6	9.4	10.0
Ni	78.2	53.3	1.1	4.4	3.1	1.9	13.1	13.6	8.1	8.9	12.8
Cu	42	12	2	7	9	49	22	17	5	11	11
Zn	93	81	10	48	46	64	76	94	87	64	65
Ga	20.9	17.0	15.6	15.1	17.4	15.1	18.0	19.1	16.6	17.7	16.0
Rb	19.4	41.4	170.7	84.7	75.0	50.3	60.1	68.7	69.1	75.3	46.5
Sr	650	434	34	239	278	316	257	538	158	365	514
Y	42.8	47.9	20.6	29.8	16.4	9.5	31.8	38.6	26.6	19.1	28.4
Zr	366	387	64	223	175	43	112	266	218	148	280
Nb	16.7	14.9	34.8	11.2	14.7	4.8	13.1	12.0	12.4	12.8	11.9
Mo	0.4	0.5	0.6	0.5	0.9	0.9	0.9	0.9	0.4	0.5	1.0
Sn	1.8	1.5	2.5	1.0	1.1	0.7	1.7	1.3	0.9	0.9	1.3
Sb	0.06	0.08	0.32	0.37	0.30	1.15	0.20	0.32	0.46	0.37	0.27
Cs	0.35	0.23	1.64	0.81	6.91	1.35	7.04	2.28	1.12	3.10	4.21
Ba	884	1081	360	1347	1978	414	1715	1135	1340	1227	700
La	33.2	34.3	16.6	27.6	28.5	23.5	83.6	28.8	32.9	29.6	28.8
Ce	81.7	88.5	71.4	56.9	55.3	44.2	85.5	64.1	47.6	55.4	62.7
Pr	10.65	9.90	4.38	6.92	6.67	4.87	15.24	8.19	7.96	6.73	7.81
Nd	44.4	40.0	15.4	25.7	24.4	17.4	58.1	32.2	29.9	24.4	29.6
Sm	9.48	8.27	3.46	4.85	4.35	2.67	9.68	6.74	5.51	4.35	5.93
Eu	2.42	2.04	0.39	1.12	1.14	0.85	2.21	1.60	1.49	1.18	1.39
Tb	1.231	1.072	0.578	0.656	0.520	0.293	1.094	0.939	0.709	0.532	0.779
Gd	8.42	7.33	3.19	4.34	3.57	2.13	8.11	6.16	4.81	3.69	5.13
Dy	7.09	6.12	3.77	3.90	2.89	1.60	5.69	5.60	4.07	3.02	4.60
Ho	1.40	1.21	0.77	0.82	0.56	0.33	1.05	1.12	0.82	0.61	0.92
Er	3.87	3.34	2.30	2.44	1.53	0.91	2.81	3.19	2.30	1.67	2.62
Yb	3.60	3.16	2.70	2.53	1.46	0.89	2.42	3.17	2.17	1.64	2.58
Lu	0.530	0.471	0.377	0.385	0.215	0.139	0.347	0.475	0.332	0.252	0.386
Hf	6.03	6.41	2.39	4.19	3.55	1.21	3.09	4.95	4.08	3.34	5.16
Ta	0.79	0.74	3.56	0.75	0.85	0.29	0.95	0.71	0.85	0.93	0.71
W	0.25	0.39	0.34	0.65	0.38	0.34	0.44	0.51	0.79	0.53	0.29
Tl	0.07	0.28	0.85	0.70	0.70	0.36	0.69	0.44	0.60	0.53	0.27
Pb	12.4	10.1	8.6	3.2	8.7	4.0	13.6	12.2	5.5	5.0	7.6
Th	2.23	2.77	26.40	7.03	5.92	5.03	8.14	4.51	6.69	8.15	4.87
U	0.49	0.62	2.46	1.99	1.19	0.47	2.05	0.94	1.84	1.97	

Note: All concentrations reported in ppm, except P reported in wt% in the form of P₂O₅. Uncertainties consider the reproducibility of standard samples according to Mori et al. (2009).

and sedimentary succession hundreds of meters thick, in which volcanic rocks become subordinate to sedimentary rocks upsection; this is most evident in southern Coahuila and northern Zacatecas (Blickwede, 1981). Coeval volcanic rocks of Early–Late Jurassic age (ca. 190–145 Ma) in Sonora (Corona, 1979; Nourse, 1995; Iriondo, 2001; Mauel et al., 2004; Anderson et al., 2005; Izaguirre-Pompa, 2009) are part of a continental Cordilleran arc that extended into California and Arizona. Late Jurassic plutons and pyroclastic rocks in southern Arizona and northern Sonora have been interpreted as primarily rift related (Haxel et al., 2008; Mauel et al., in press).

Jones et al. (1995) proposed that the Nazas assemblage of the Mexican Altiplano represents a fragment of the Sonoran part of the arc that was displaced hundreds of kilometers southeast along a hypothetical left-lateral strike-slip fault, but convincing evidence was presented against this model by Molina-Garza and Geissman (1999) and Barboza-Gudiño

et al. (2008). Jurassic volcanic arc rocks of the Nazas Formation overlie strata of the Late Triassic Potosí fan (Silva-Romo et al., 2000; Barboza-Gudiño et al., 2008), which contains zircons derived from the East Mexico arc, Pan-African rocks, and Grenvillian basement; rocks of the Potosí fan do not contain southwestern North America-derived zircons (1.6–1.8 Ga; Barboza-Gudiño, 2008). It is thus unlikely that rocks of the Nazas Formation were formed near present-day Sonora.

Early–Middle Jurassic magmatism has been reported for localities in southern Mexico such as the Las Lluvias ignimbrite in Guerrero (Campa-Uranga et al., 2004) and the San Felipe granite in Oaxaca (Alaniz-Alvarez et al., 1996). The relationship of these rocks to the Nazas arc is uncertain, but it is generally assumed that they were produced adjacent to the same subduction system; some have suggested that the Nazas arc was continuous with the Jurassic arc of northwestern South America (e.g., Dickinson and Lawton, 2001).

Nazas continental arc volcanism is clearly pre-Oxfordian and spans the Early and Middle Jurassic. Nazas strata underlie the La Joya Formation or the Oxfordian Zuloaga Formation (Barboza-Gudiño et al., 2004). There are ages as old as 198 ± 7 Ma (K-Ar in Santa María el Oro, Durango; Damon et al., 1981), 189 Ma at Huizachal Canyon in Tamaulipas (Fastovsky et al., 2005), 172.5 ± 5.1 Ma at Real de Catorce in San Luis Potosí (Barboza-Gudiño et al., 2004), 193 Ma at Aramberri in Nuevo León (Barboza-Gudiño et al., 2008), and 179 Ma at Las Lluvias in Guerrero (Campa-Uranga et al., 2004). Detrital zircon ages from the Huizachal Group in Valle Huizachal (Huizachal Canyon), Tamaulipas, contain a Jurassic grain population ranging from ca. 199 to 160 Ma, nearly identical to the age range of the Early–Middle Jurassic population of our El Diamante sample and similarly indicate the temporal span of pre-rift volcanism (Rubio-Cisneros and Lawton, in press).

The outcrop belt of the Nazas Formation trends at an azimuth of ~300° from Durango

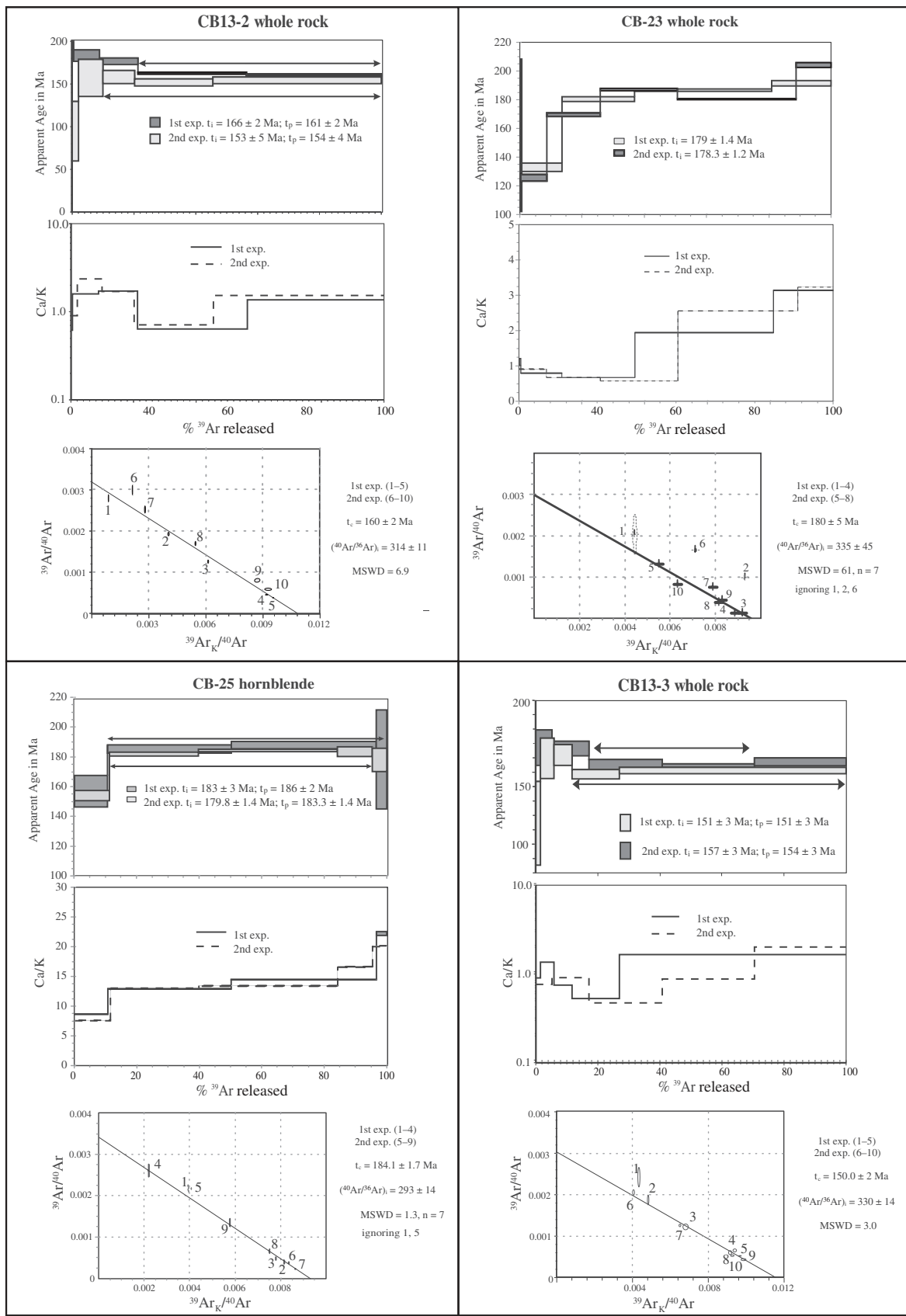


Figure 9. $^{40}\text{Ar}-^{39}\text{Ar}$ data for Custepéc dikes of the Chiapas massif. The symbols t_p and t_i correspond to plateau and integrated age, respectively. MSWD—mean square of weighted deviates.

TABLE 3. U-Th-Pb ANALYTICAL DATA FOR SHRIMP (SENSITIVE HIGH-RESOLUTION ION MICROPROBE) SPOT ANALYSES ON ZIRCON GRAINS FROM LA SILLA FORMATION DACITE, SOUTHERN MEXICO

Spot Name	Comments Core/Rim?	Common ^{206}Pb (%)	U (ppm)	Th (ppm)	Th/U	$^{238}\text{U}/^{206}\text{Pb}^*$	error (%)	$^{207}\text{Pb}/^{206}\text{Pb}^*$	error (%)	$^{208}\text{Pb}/^{238}\text{U}^*$	error (%)	$^{206}\text{Pb}/^{238}\text{U}^*$	Age (Ma)	error (Ma)
Sample VC-4	dacite (southern Mexico)	Mount Alex-20												
M752-2	Rim	0.31	21	20	1.02	34.1665	± 3.2337	0.0522	± 8.7353	0.0292	± 0.0010	185.4	± 6.0	
M752-3	Core	0.12	38	34	0.94	34.1902	± 2.6788	0.0508	± 6.6932	0.0292	± 0.0008	185.6	± 5.0	
M752-9	Core	-0.26	31	42	1.40	34.0688	± 2.8105	0.0477	± 8.3122	0.0294	± 0.0008	187.0	± 5.3	
M752-5	Core	0.64	25	32	1.31	33.6053	± 3.0323	0.0550	± 9.1983	0.0296	± 0.0009	187.8	± 5.8	
M752-7	Core	-0.04	42	59	1.44	33.8273	± 2.5906	0.0495	± 6.2382	0.0296	± 0.0008	187.9	± 4.9	
M752-1	Core	-0.15	57	83	1.51	33.4652	± 2.3964	0.0487	± 5.3087	0.0299	± 0.0007	190.1	± 4.6	
M752-11	Core-rim	-0.32	92	57	0.63	33.3144	± 2.1675	0.0474	± 6.3248	0.0301	± 0.0007	191.3	± 4.2	
M752-6	Core	0.03	24	34	1.44	32.8459	± 3.0300	0.0502	± 7.9602	0.0304	± 0.0009	193.3	± 5.9	
M752-10	Core	-0.56	28	27	1.00	32.3673	± 2.8621	0.0456	± 7.7510	0.0311	± 0.0009	197.2	± 5.7	
M752-4	Core	-0.14	43	52	1.24	32.1841	± 2.5657	0.0489	± 6.1865	0.0311	± 0.0008	197.5	± 5.1	
M752-12	Core	-1.05	30	34	1.17	32.2115	± 2.7878	0.0417	± 7.6909	0.0314	± 0.0009	199.1	± 5.6	
M752-8	Core-rim	-0.23	111	97	0.90	24.5333	± 2.0718	0.0495	± 3.3189	0.0409	± 0.0009	258.1	± 5.3	
(MSWD = 0.85, n = 11)												Mean $^{206}\text{Pb}/^{238}\text{U}$ age = 191.0 ± 3.0		

*Uncorrected atomic ratios.

#Atomic ratios and ages corrected for initial Pb using the amount of ^{207}Pb .

Individual zircon ages in bold were used to calculate the weighted average $^{206}\text{Pb}/^{238}\text{U}$ age and its MSWD (mean square of weighted deviates).

All errors given are at the 1 sigma level except for the weighted average $^{206}\text{Pb}/^{238}\text{U}$ age reported at 2 sigma.

in the west to Huizachal Canyon in the east (Fig. 10). It appears to be continuous beneath volcanic cover of the Sierra Madre Occidental with the Cordilleran arc to the northwest. South of the Nazas arc we recognize a belt of Early to Middle Jurassic marine strata (Fig. 10), from the Pelayo Formation in Chihuahua (Franco-Rubio et al., 2007) to the Huayacocota Formation in Hidalgo (Ochoa-Camarillo et al., 1998). This belt is discontinuous in comparison to the Nazas outcrop belt (Fig. 10), but it appears to project into Lower–Middle(?) Jurassic marine strata of the Sierra Santa Rosa Formation of northwest Sonora (González-León et al., 2000).

If the Maya block is rotated ~35° about the Euler pole of Hall and Najmuddin (1994) to restore it to its preopening position (between ca. 195 and 160 Ma), outcrops of volcanic rocks of the La Silla Formation on the eastern flank of the Chiapas massif constitute an eastward continuation of the Nazas arc (Fig. 10). This restoration, together with the observations of volcanic arc chemistry and similar age range, suggests to us that the La Silla and Nazas Formations originated as parts of the same arc system.

We schematically trace a trench along western Mexico ~350 km from the trend of the Cordilleran–Nazas–La Silla belt and subparallel to it (Fig. 10). We reconstructed the margin of South America according to Pindell et al. (2006) ca. 170 Ma, following the southeastward relative motion of South and North America. Two conclusions follow from this reconstruction. First, the trench associated with the Nazas arc must have turned abruptly south to avoid the South America margin and produce Jurassic magmatism in the northern Andes (Mojica et al., 1996). Second, in the reconstruction South America overlaps with Precambrian and Paleozoic crust of the southern Mexico terranes of Oaxaca and

Acatlán, implying that either Oaxaca–Acatlán or the Colombian Andes were located elsewhere (e.g., Bayona et al., 2006). The reconstruction of the northern margin of South America suggests that the trench must turn sharply southward, as illustrated in Figure 10. Such an abrupt turn can be observed in current plate configurations, such as the Aleutian–Kamchatka trench juncture.

When the Oaxaca and Acatlán terranes of southern Mexico arrived to their present position is debated. Secondary magnetizations in Paleozoic strata have been interpreted as a late Paleozoic overprint yielding a paleopole that agrees with the Late Permian reference pole of North America (McCabe et al., 1988). This suggests that by Permian time, the Oaxaca terrane had arrived at its present position. However, paleomagnetic data for Jurassic strata in the Acatlán terrane have been interpreted to indicate allochthonity in Middle Jurassic time (Bohnel, 1999). The strongest argument for locating Acatlán and Oaxaca at a different location than present with respect to the craton is still the overlap with the reconstructed margin of South America based on magnetic anomalies and fracture zones of the Atlantic (Pindell et al., 2006). Nonetheless, based on paleomagnetic data, Bayona et al. (2006) suggested a more southern paleolatitude for the Colombian Andes. In the reconstruction of Figure 10 this issue remains unresolved.

In summary, the La Silla Formation represents arc-related volcanic rocks of Sinemurian–Pliensbachian age. Although the presence of Middle Jurassic magmatism was recognized previously (Castro-Mora et al., 1975), we document its relationship to subduction and the fact that this magmatism is widespread in Chiapas. The El Diamante Member of the Todos Santos Formation represents continental strata and subordinate volcanic flows deposited in an intra-arc

extensional basin transitional to a rift setting. It is possible that the youngest dike ages could represent extension-related magmatism, but available data are insufficient to support this interpretation. The suprajacent Jericó Member records continental rifting after cessation of magmatism. The uppermost Todos Santos and San Ricardo Formations are interpreted to record the drift phase of the Maya block and subsequent thermal subsidence.

CONCLUSIONS

The Jurassic stratigraphy of central Chiapas directly overlies and onlaps plutonic and metamorphic basement of the Chiapas massif, and consists of an Early–Middle Jurassic assemblage of intermediate calc-alkaline volcanic flows and related dikes termed the La Silla Formation, overlain by Upper Jurassic sedimentary strata termed the Todos Santos Formation. The lower member of the Todos Santos Formation, referred to as the El Diamante Member, consists of mudstone-dominated red-beds deposited by a sinuous river system and subordinate basaltic andesite flows. Sandstone petrology indicates a volcanic lithic composition, and effectively unimodal detrital zircon ages demonstrate derivation from subjacent Early–Middle Jurassic volcanic rocks. The upper member of the Todos Santos Formation, referred to here as the Jericó Member, consists of deposits of large sandy rivers containing arkosic detritus derived from Permian–Triassic, Paleozoic, and Proterozoic crystalline and metasedimentary rocks of the Chiapas massif.

U-Pb geochronology provides a direct age of 191 Ma for the La Silla Formation volcanics. $^{40}\text{Ar}/^{39}\text{Ar}$ ages on dikes, some of which may be genetically related to the La Silla volcanic

TABLE 4. SUMMARY OF ^{40}Ar - ^{39}Ar RESULTS

CB13-2 whole-rock MS-10 temperature controlled step-heating experiments; J = 0.004675 ± 0.0000027											
Temp	^{39}Ar (F)	$^{40}\text{Ar}^{*}/^{39}\text{Ar}_{\text{K}}$	t	$^{40}\text{Ar}^{*}$ (%)	$^{40}\text{Ar}/^{39}\text{Ar}$	t_i	^{39}Ar (%)	MSWD/n	t_c	$(^{40}\text{Ar}/^{39}\text{Ar})_i$	MSWD/n
600	0.0049	42.61 ± 6.71	327.8 ± 47.2	17.41	357.79	0.617					
800	0.0833	22.86 ± 0.88	183.2 ± 6.7	43.10	519.30	1.593					
900	0.1245	22.00 ± 0.50	176.6 ± 5.0	62.88	795.97	1.716					
1050	0.3509	20.18 ± 0.14	162.6 ± 1.1	86.67	2216.01	0.637					
1350	0.4365	19.92 ± 0.13	160.6 ± 1.0	88.76	2630.10	1.364					
700	0.0205	11.52 ± 4.36	94.7 ± 34.9	11.50	333.91	0.902					
800	0.0789	19.46 ± 2.81	157.1 ± 21.7	25.43	396.28	2.359					
900	0.1025	19.59 ± 0.99	158.1 ± 7.7	49.90	589.83	1.698					
1050	0.2532	18.77 ± 0.53	151.8 ± 4.1	76.32	1247.90	0.710					
1350	0.5449	19.10 ± 0.50	154.3 ± 3.9	82.73	1711.42	1.530	153.1 ± 4.9	153.7 ± 2.0	98.0	0.2 / 4	158.3 ± 2.4
CB13-3 whole-rock MS-10 temperature controlled step-heating experiments; J = 0.004578 ± 0.0000034											
Temp	^{39}Ar (F)	$^{40}\text{Ar}^{*}/^{39}\text{Ar}_{\text{K}}$	t	$^{40}\text{Ar}^{*}$ (%)	$^{40}\text{Ar}/^{39}\text{Ar}$	t_i	^{39}Ar (%)	MSWD/n	t_c	$(^{40}\text{Ar}/^{39}\text{Ar})_i$	MSWD/n
700	0.0151	14.31 ± 3.75	114.5 ± 29.1	28.41	412.79	0.902					
800	0.0435	20.21 ± 1.86	159.6 ± 14.0	44.64	533.79	1.358					
900	0.0583	20.51 ± 0.92	161.9 ± 7.2	63.88	818.08	0.749					
1050	0.1525	18.75 ± 0.43	148.6 ± 3.3	80.65	1526.90	0.528					
1350	0.7306	19.09 ± 0.29	151.1 ± 2.2	84.54	1910.99	1.652					
800	0.0522	21.19 ± 1.64	167.0 ± 12.3	39.31	486.89	0.763					
900	0.1191	21.11 ± 0.67	166.4 ± 5.1	62.83	794.96	0.908					
1050	0.2362	19.62 ± 0.48	155.2 ± 3.6	82.20	1660.02	0.472					
1150	0.2971	19.32 ± 0.38	152.9 ± 2.9	87.21	2309.99	0.877					
1350	0.2953	19.88 ± 0.36	157.2 ± 2.7	84.37	1890.44	2.011	157.0 ± 3.2	154.9 ± 1.6	82.9	1.3 / 3	149.1 ± 2.4
CB21c groundmass GS5400 laser step-heating experiments; J = 0.003641 ± 0.000006											
Pot	^{39}Ar (F)	$^{40}\text{Ar}^{*}/^{39}\text{Ar}_{\text{K}}$	t	$^{40}\text{Ar}^{*}$ (%)	$^{40}\text{Ar}/^{39}\text{Ar}$	t_i	^{39}Ar (%)	MSWD/n	t_c	$(^{40}\text{Ar}/^{39}\text{Ar})_i$	MSWD/n
0.20	0.0128	66.84 ± 3.00	393.0 ± 15.9	‡	66.31	877.10	3.156				
0.30	0.0213	18.72 ± 1.13	119.0 ± 6.9	‡	61.98	777.30	6.916				
0.60	0.1533	149.6 ± 0.36	149.6 ± 2.2	‡	87.79	2419.61	6.462				
0.80	0.1619	23.59 ± 0.22	148.7 ± 1.3	‡	97.59	12281.85	2.017				
1.00	0.2259	24.22 ± 0.16	152.5 ± 1.0	‡	97.31	10968.36	2.135				
1.20	0.0829	24.63 ± 0.25	154.9 ± 1.5	‡	97.59	12279.24	5.248				
1.60	0.1386	25.03 ± 0.24	157.3 ± 1.4	‡	96.11	7587.50	6.307				
2.00	0.0799	24.95 ± 0.26	156.9 ± 1.6	‡	94.69	5567.29	4.140				
CB23 whole-rock MS-10 temperature controlled step-heating experiments; J = 0.005032 ± 0.0000033											
Temp	^{39}Ar (F)	$^{40}\text{Ar}^{*}/^{39}\text{Ar}_{\text{K}}$	t	$^{40}\text{Ar}^{*}$ (%)	$^{40}\text{Ar}/^{39}\text{Ar}$	t_i	^{39}Ar (%)	MSWD/n	t_c	$(^{40}\text{Ar}/^{39}\text{Ar})_i$	MSWD/n
600	0.0068	17.87 ± 6.38	155.3 ± 53.1	‡	39.91	491.78	1.118				
800	0.1296	15.20 ± 0.34	133.0 ± 2.8	‡	70.99	1018.59	0.795				
950	0.2321	20.92 ± 0.19	180.5 ± 1.6	‡	96.52	8502.80	0.667				
1100	0.4415	21.66 ± 0.11	186.6 ± 0.9	‡	96.48	8395.53	1.942				
1350	0.1900	22.26 ± 0.24	191.4 ± 2.0	‡	61.47	766.98	3.145				
800	0.0868	14.33 ± 0.28	125.1 ± 2.3	‡	51.29	606.66	9.091				
900	0.1714	19.61 ± 0.14	169.4 ± 1.2	‡	77.64	1321.38	6.769				
1000	0.2476	21.73 ± 0.09	187.4 ± 0.7	‡	88.89	2658.80	5.752				
1200	0.3823	20.92 ± 0.06	180.5 ± 0.5	‡	87.14	2298.49	2.557				
1350	0.1119	23.82 ± 0.22	204.2 ± 1.8	‡	75.67	12194.63	3.230				
CB25 hornblend MS-10 temperature controlled step-heating experiments; J = 0.005030 ± 0.0000033											
Temp	^{39}Ar (F)	$^{40}\text{Ar}^{*}/^{39}\text{Ar}_{\text{K}}$	t	$^{40}\text{Ar}^{*}$ (%)	$^{40}\text{Ar}/^{39}\text{Ar}$	t_i	^{39}Ar (%)	MSWD/n	t_c	$(^{40}\text{Ar}/^{39}\text{Ar})_i$	MSWD/n
1050	0.1068	18.05 ± 1.27	156.8 ± 10.6	‡	35.80	460.29	8.68				
1150	0.3985	21.50 ± 0.34	185.3 ± 2.8	‡	88.21	2507.16	12.90				
1250	0.4642	21.83 ± 0.30	188.0 ± 2.4	‡	85.55	2045.67	14.44				
1350	0.0335	20.65 ± 4.04	178.3 ± 33.2	‡	22.92	383.36	22.22				
1050	0.1147	17.73 ± 0.41	154.1 ± 3.4	‡	36.29	463.82	7.60				
1150	0.2842	21.07 ± 0.16	181.8 ± 1.3	‡	88.64	2602.03	13.02				
1200	0.4434	21.39 ± 0.11	184.4 ± 0.9	‡	93.02	4236.30	13.39				
1275	0.1116	21.26 ± 0.40	183.3 ± 3.2	‡	80.44	1510.57	16.61				
1350	0.0462	20.62 ± 0.95	178.1 ± 7.8	‡	59.92	737.19	20.09				

Note: MSWD—mean square of weighted deviates; F—fraction; Temp—the temperature reached in the Ta furnace at which the argon was released; Pot—laser power (in watts) applied to release argon; t—age of individual fraction, it does not include the uncertainty in J; t_i —integrated age; t_p —plateau age calculated with the weighted mean of the fractions selected; t_s —sochron age; \bar{s} —fractions used to calculate the plateau age; \pm —fractions ignored in the sochron age calculation; \dagger —isochron age calculated combining the fractions of the experiments performed for sample; all errors are given to 1σ level. Preferred age is highlighted in bold typeface.

TABLE 5. SUMMARY OF ^{40}Ar - ^{39}Ar FOR JURASSIC DIKES OF THE CHIAPAS MASSIF

Sample	Coordinates	1st experiment (Ma)	2nd experiment (Ma)	Isochron age (Ma)	MSWs- ^{40}Ar / ^{36}Ar
CB25	16.5637°N, 92.6459°W	186 ± 2	183.2 ± 1.4	184.1 ± 1.7	1.3
Nueva Palestina					293 ± 14
CB23	16.0431°N, 93.4055°W	179.0 ± 1.4	178.3 ± 1.2	180.0 ± 5	61
Monterrey					334 ± 45
CB13-2	16.3342°N, 93.2611°W	161 ± 2	154 ± 4	160 ± 2	6.9
Villa Flores					314 ± 11
CB13-3	16.3342°N, 93.2611°W	151 ± 3	154 ± 3	150 ± 2	3.0
Villa Flores					330 ± 14
CB21c	15.78646°N, 92.94653°W	153 ± 3	148 ± 2	146 ± 4	2.0
Custepec					740 ± 233

Note: MSWDs—mean square of weighted deviations.

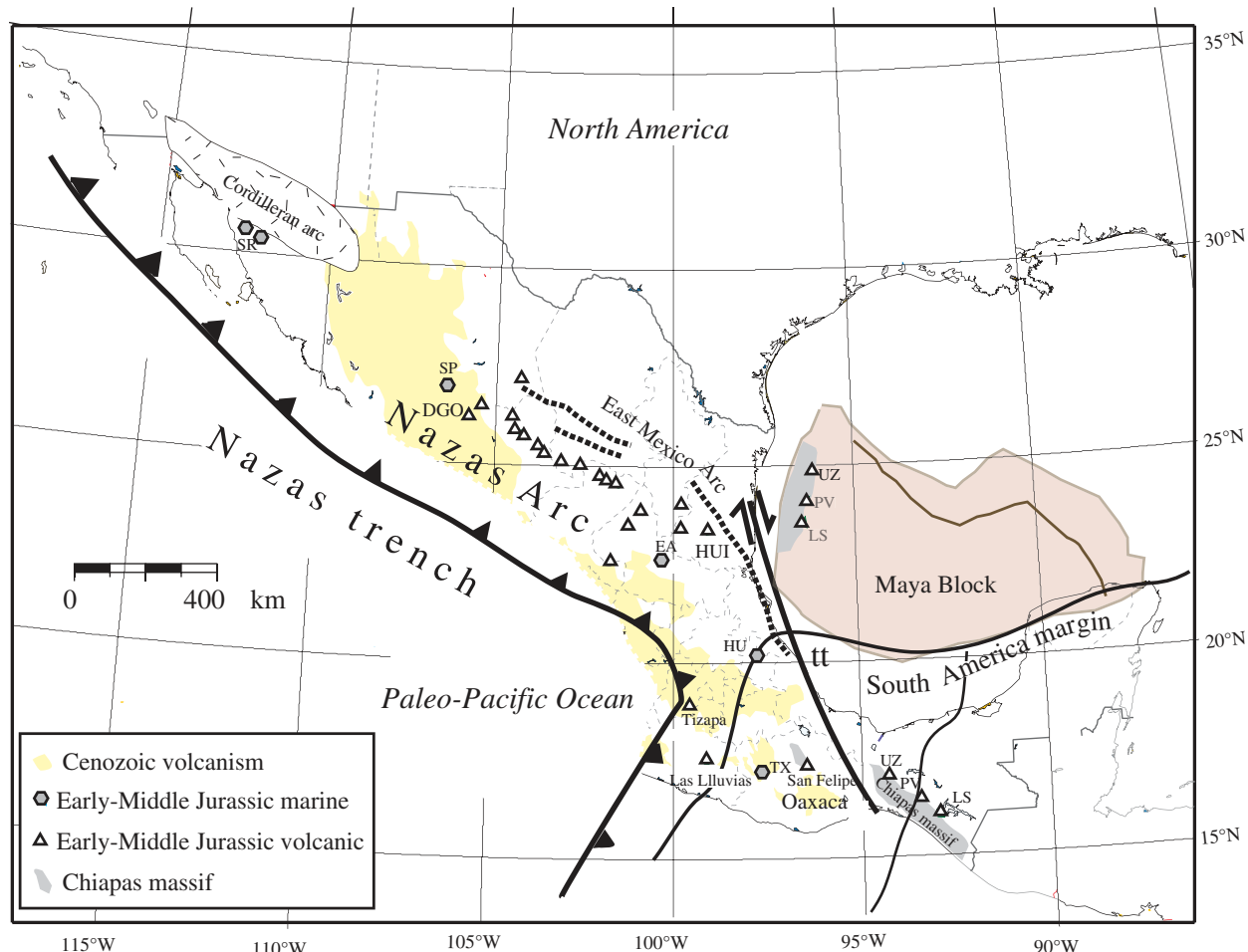


Figure 10. Reconstruction of the Gulf of Mexico region and the Nazas arc for ca. 195–165 Ma. The trend of the arc extends from its type locality in Durango (DGO) to its easternmost exposure at Huizachal canyon (HUI). Other symbols are Early to Middle Jurassic marine localities: SR—Sierra Santa Rosa, Sonora; SP—Pelayo Formation, Olivos valley, Chihuahua; EA—El Alamito, San Luis Potosí; HU—Huayacocotla, Puebla. Symbols for other localities mentioned in the text: PV—Pueblo Viejo, Chiapas; LS—La Silla, Chiapas; UZ—Uzpanapa; tt—Chiapas-Tamaulipas transform; TX—Tlaxiaco Basin.

rocks, indicate an age range of 184–150 Ma. Trace element analysis demonstrates that the La Silla volcanic rocks have characteristics of typical subduction-related melts and thus provide a record of Early–Middle Jurassic arc magmatism.

The Jurassic succession in Chiapas records: (1) the development and demise of

an Early–Middle Jurassic continental arc; (2) an early-Late Jurassic transition through an intra-arc basin in which the El Diamante Member was deposited; and (3) subsequent development of a Late Jurassic continental rift, evidenced by deposition of Jericó Member fluvial and alluvial fan deposits, which

directly overlie both the Chiapas massif and the older Jurassic arc volcanic rocks. Rift-basin development yielded to deposition of more widespread Kimmeridgian strata attributed to post-rift thermal subsidence in Chiapas, coeval with opening of the Gulf of Mexico Basin.

APPENDIX. PETROGRAPHIC DESCRIPTION OF VOLCANIC ROCKS

According to their texture, volcanic rocks of La Silla Formation were arranged in three groups that correspond to different modal compositions. Group 1 is characterized by porphyric textures. Phenocrysts present disequilibrium textures, as they occur as corroded, reabsorbed, and skeletal grains. According to phenocryst composition, we recognized a subgroup that included sites 2, 14, 18 and 20, which in addition to plagioclase and K-feldspar phenocrysts, presents hornblende and minor pyroxene (Fig. A1). Plagioclase is more abundant than K-feldspar with typical

modal compositions of 60–70% plagioclase, 25–30% K-feldspar, 15% hornblende, and <5% pyroxene. Amphiboles are represented by skeletal hornblende nearly completely replaced by opaque minerals. Feldspars are typically dusty due to secondary sericitic. These rocks are classified as hornblende dacites. Also with porphyritic texture, site VC1 is characterized by relatively more abundant K-feldspar than plagioclase, and is classified as a hornblende rhyodacite.

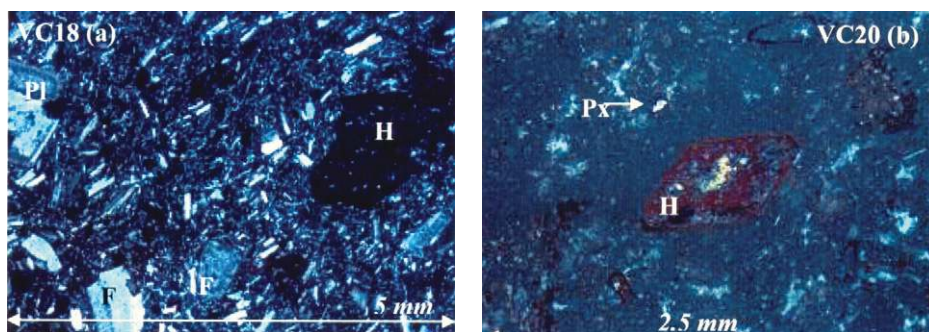


Figure A1. (A) (left) Cross-nichols photomicrograph of sample from site VC18. H—hornblende, Pl—plagioclase, F—K-feldspar. (B) VC20 shows hornblende and pyroxene phenocrysts.

The second group includes sites with pervasive flow bands, with dark bands concentrating opaque minerals and microphenocrysts. It includes sites 3, 4, and 29. These rocks typically present devitrified matrix partially replaced by reddish oxides, containing phenocrysts of plagioclase, K-feldspar, and minor quartz.

Skeletal pyroxene is also present as phenocrysts. Modal abundances of phenocrysts are 70–80% plagioclase, 10–15% K-feldspar, 10% hornblende, 5% pyroxene, and 5% quartz in VC3. They are classified as hornblende-pyroxene andesites (Fig. A2).

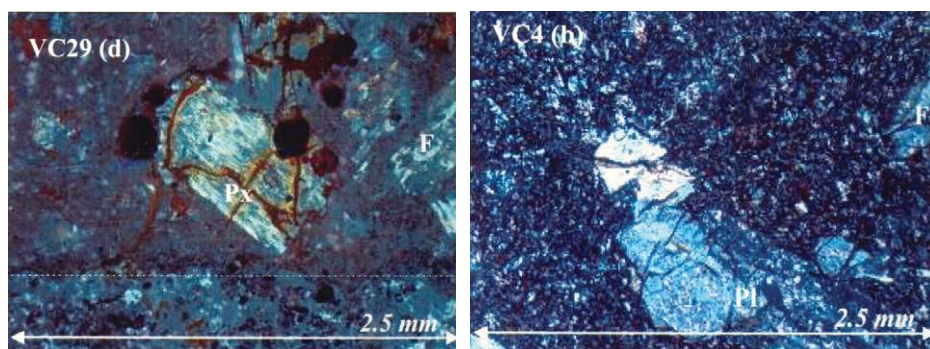


Figure A2. (A) (left) Cross-nichols photomicrograph of a sample from site VC4; symbols as in Figure A1. (B) a pyroxene phenocryst and banding indicated by dotted line.

Finally, a third group of samples presents amygdaloidal textures. It includes sites VC10 (85% plagioclase and 15% olivine; an olivine basalt), and site VC11 (95% plagioclase, 5% hornblende; a hornblende basalt). Olivine is completely altered to iddingsite. Amygdules are of nearly spherical morphology, and the great majority is

lined by zeolite. The matrix contains abundant acicular plagioclase, giving the rock a tenuous pilotaxitic texture. The matrix shows intense oxidation, with pigmentary hematite replacing original ferromagnesian phases. Site 10 is the stratigraphically highest volcanic rock, and is included in the Todos Santos Formation.

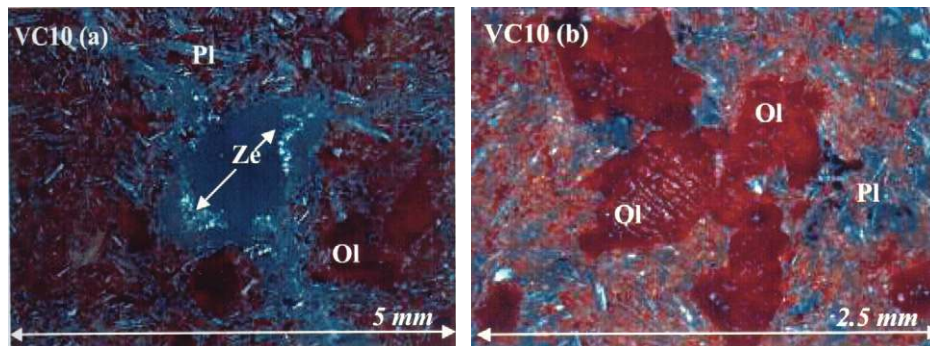


Figure A3. (A) (left) and (B) are cross-nichols photomicrographs of olivine basalt from site VC10. Ol—olivine (iddingsite), Ze—zeolite.

ACKNOWLEDGMENTS

Partial funding for mineral separations and detrital zircon analyses was provided by a Fulbright-Garcia Robles Research Fellowship and the Manasse Endowed Chair, College of Arts and Sciences, New Mexico State University, to Lawton. Partial funding from Universidad Nacional Autónoma de México-PAPIIT (Programa de Apoyo a Proyectos de Investigación e Innovación Tecnológica) project IN121002 to Molina-Garza is acknowledged. Iriondo thanks Joe Wooden and Wayne Premo from the U.S. Geological Survey for their help and supervision while running the SHRIMP-RG at Stanford University, and Pedro Castañeras, a former University of Colorado postdoctoral fellow, for help preparing the zircon mount for the U-Pb studies. We also thank Bob Stern for his review.

REFERENCES CITED

- Alaniz-Alvarez, S.A., van der Heyden, P., Nieto Samaniego, A.F., and Ortega-Gutiérrez, F., 1996, Radiometric and kinematic evidence for Middle Jurassic strike-slip faulting in southern Mexico related to the opening of the Gulf of Mexico: *Geology*, v. 24, p. 443–446, doi: 10.1130/0091-7613(1996)024<443:RAKEFM>2.0.CO;2.
- Alencaster, G., 1977, Moluscos y braquiópodos del Jurásico Superior de Chiapas: Instituto de Geología, Universidad Nacional Autónoma de México, Revista, v. 1, p. 151–166.
- Anderson, T.H., Burkart, B., Clemons, R.E., Bohnenberger, O.H., and Blount, D.N., 1973, Geology of the Western Altos Cuchumatanes, northwestern Guatemala: Geological Society of America Bulletin, v. 84, p. 805–826, doi: 10.1130/0016-7606(1973)84<805:GOTWAC>2.0.CO;2.
- Anderson, T.H., Rodriguez-Castañeda, J.L., and Silver, L.T., 2005, Jurassic rocks in Sonora, Mexico: relations to the Mojave-Sonora megashear and its inferred northward extension, in Anderson, T.H., et al., eds., The Mojave-Sonora megashear hypothesis: development, assessment, and alternatives: Geological Society of America Special Paper 393, p. 51–95, doi: 10.1130/0-8137-2393-0.51.
- Arvizu, H.E., Iriondo, A., Izaguirre, A., Chávez-Cabello, G., Kamenov, G.D., Solís-Pichardo, G., Foster, D.A., and Lozano-Santa Cruz, R., 2009, Rocas graníticas pérmicas en la Sierra Pinta, NW de Sonora, México: Magmatismo de subducción asociado al inicio del margen continental activo del SW de Norteamérica: *Revista Mexicana de Ciencias Geológicas*, v. 26, p. 709–728.
- Barboza-Gudiño, J.R., 2008, Detrital-zircon geochronology of Triassic fluvial and submarine fan deposits from northeastern Mexico: Stratigraphy, paleogeography and tectonic implications: Geological Society of America Abstracts with Programs, v. 40, no. 6, p. 197.
- Barboza-Gudiño, J.R., Tristán González, M., and Torres Hernández, J.R., 1998, The Late Triassic-Early Jurassic active continental margin of western North America in northeastern Mexico: *Geofísica Internacional*, v. 37, p. 283–292.
- Barboza-Gudiño, J.R., Hoppe, M., Gómez-Anguiano, M., and Martínez-Macías, P.R., 2004, Aportaciones para la interpretación estratigráfica y estructural de la porción noroccidental de la Sierra de Catorce, San Luis Potosí, México: *Revista Mexicana de Ciencias Geológicas*, v. 21, p. 299–319.
- Barboza-Gudiño, J.R., Orozco-Esquivel, M.T., Gómez-Anguiano, M., and Zavala-Monsiváis, A., 2008, The early Mesozoic volcanic arc of western North America in northeastern Mexico: *Journal of South American Earth Sciences*, v. 25, p. 49–63, doi: 10.1016/j.jss.2007.08.003.
- Bayona, G., Rapalini, A., and Costanzo-Alvarez, V., 2006, Paleomagnetism in Mesozoic rocks of the northern Andes and its implications in Mesozoic tectonics of northwestern South America: *Earth, Planets, and Space*, v. 58, p. 1255–1272.
- Bird, D.E., Burke, K., Hall, S.A., and Casey, J.F., 2005, Gulf of Mexico tectonic history: Hotspot tracks, crustal boundaries, and early salt distribution: *American Association of Petroleum Geologists Bulletin*, v. 89, p. 311–328, doi: 10.1306/10280404026.
- Blair, T.C., 1987, Tectonic and hydrologic controls on cyclic alluvial fan, fluvial, and lacustrine rift-basin sedimentation, Jurassic-lowermost Cretaceous Todos Santos Formation, Chiapas, Mexico: *Journal of Sedimentary Petrology*, v. 57, p. 845–862, doi: 10.1306/212F8C83-2B24-11D7-8648000102C1865D.
- Blickwede, J.F., 1981, Stratigraphy and petrology of Triassic (?) Nazca Formation, Sierra de San Julian, Zacatecas, Mexico [M.S. thesis]: New Orleans, Louisiana, University of New Orleans, 100 p.
- Bohnel, H., 1999, Paleomagnetic study of Jurassic and Cretaceous rocks of the Mixteca terrane (Mexico): *Journal of South American Earth Sciences*, v. 12, p. 545–556, doi: 10.1016/S0895-9811(99)00038-3.
- Burkart, B., Clemons, R.E., and Crane, D.C., 1973, Mesozoic and Cenozoic stratigraphy of southeastern Guatemala: *American Association of Petroleum Geologists Bulletin*, v. 57, p. 63–73.
- Campa-Uranga, M.F., García-Díaz, J.L., and Iriondo, A., 2004, El arco sedimentario del Jurásico Medio (Grupo Tecocoyuncas y Las Lluvias) de Olinalá, Guerrero: GEOS: Unión Geofísica Mexicana, v. 24, p. 174.
- Castro-Mora, J., Schlaepfer, C.J., and Rodríguez, E.M., 1975, Estratigrafía y microfacies del Mesozoico de la Sierra Madre del Sur, Chiapas: Asociación Mexicana Geólogos Petroleros Boletín, v. 27, p. 1–95.
- Cerca-Martínez, M., Aguirre-Díaz, G.J., and Martínez-López, M., 2000, The geologic evolution of southern sierra de Guanajuato, Mexico: A documented example from the transition from Sierra Madre Occidental to the Mexican Volcanic Belt: *International Geology Review*, v. 42, p. 131–151, doi: 10.1080/00206810009465073.
- Clemons, R.E., Anderson, T.H., Bohnenberger, O.H., and Burkart, B., 1974, Stratigraphic nomenclature of recognized Paleozoic and Mesozoic rocks of western Guatemala: *American Association of Petroleum Geologists Bulletin*, v. 58, p. 313–320.
- Consejo de Recursos Minerales, 1994, Mapa Geológico Estado de Chiapas: Pachuca, Mexico, Consejo de Recursos Minerales, scale 1:500,000.
- Corona, F.V., 1979, Preliminary reconnaissance geology of Sierra La Gloria and Cerro Basura, northwestern Sonora, Mexico, in Anderson, T.H., and Roldán-Quijano, J., eds., Geology of northern Sonora: Geological Society of America Field Trip 27 Guidebook: Pittsburgh, Pennsylvania, University of Pittsburgh, p. 59–69.
- Damon, P.E., Shafiqullah, M., and Clark, K.F., 1981, Age trends of igneous activity in relation to metallogenesis in the southern Cordillera, in Dickinson, W.R., and Payne, W.D., eds., Relations of tectonics to ore deposits in the southern Cordillera: Arizona Geological Society Digest, v. 14, p. 137–154.
- Dickinson, W.R., and Gehrels, G.E., 2009, Use of U-Pb ages of detrital zircons to infer maximum depositional ages of strata: A test against a Colorado Plateau Mesozoic database: *Earth and Planetary Science Letters*, v. 288, p. 115–125, doi: 10.1016/j.epsl.2009.09.013.
- Dickinson, W.R., and Lawton, T.F., 2001, Carboniferous to Cretaceous assembly and fragmentation of Mexico: *Geological Society of America Bulletin*, v. 113, p. 1142–1160, doi: 10.1130/0016-7606(2001)113<1142:CTCAAF>2.0.CO;2.
- Exxon, 1985, Tectonic map of the world: Houston, Texas, Exxon Production Research Company World Mapping Project, American Association of Petroleum Geologists.
- Fastovsky, D.E., Hermes, O.D., Strater, N.H., Bowring, S.A., Clark, J.M., Montellano, M., and Hernandez, R.P., 2005, Pre-Late Jurassic, fossil-bearing volcanic and sedimentary red beds of Huizachal Canyon, Tamaulipas, Mexico, in Anderson, T.H., et al., eds., The Mojave-Sonora megashear hypothesis: development, assessment, and alternatives: Geological Society of America Special Paper 393, p. 401–426, doi: 10.1130/0-8137-2393-0.401.
- Franco-Rubio, M., Comaduran-Ahumada, O., Alva-Valdivia, L.M., Urrutia-Fucugauchi, J., and Molina Garza, R.S., 2007, The Olivos olistostrome: remnant of a Late Permian oceanic basin along the southwestern margin of Laurentia, Chihuahua, Mexico: *International Geology Review*, v. 49, p. 1127–1144, doi: 10.2747/0020-6814.49.12.1127.
- Gehrels, G.E., Valencia, V.A., and Ruiz, J., 2008, Enhanced precision, accuracy, efficiency, and spatial resolution of U-Pb ages by laser ablation–multicollector-inductively coupled plasma–mass spectrometry: *Geochemistry, Geophysics, Geosystems*, v. 9, Q03017, 13 p., doi: 10.1029/2007GC001805.
- Goldammer, R.K., 1999, Mesozoic sequence stratigraphy and paleogeographic evolution of northeast Mexico, in Bartolini, C., et al., eds., Mesozoic sedimentary and tectonic history of north-central Mexico: Geological Society of America Special Paper 340, p. 1–58, doi: 10.1130/0-8137-2340-X.1.
- González-León, C.M., Stanley, G.D., Jr., and Taylor, D.G., 2000, Ammonoid discoveries in the Antimorio Formation, Sonora, Mexico: New constraints on the Triassic-Jurassic boundary: *Journal of South American Earth Sciences*, v. 13, p. 491–497, doi: 10.1016/S0895-9811(00)00038-9.
- Gose, W.A., and Finch, R.C., 1992, Stratigraphic implications of palaeomagnetic data from Honduras: *Geophysical Journal International*, v. 108, p. 855–864, doi: 10.1111/j.1365-246X.1992.tb03475.x.
- Guerrero, J.C., Herrero-Bervera, E., and Helsley, C.E., 1990, Paleomagnetic evidence for post-Jurassic stability of southeastern Mexico: Maya terrane: *Journal of Geophysical Research*, v. 95, p. 7091–7100, doi: 10.1029/JB095iB05p07091.
- Hall, S.A., and Najmuddin, I.J., 1994, Constraints on the tectonic development of the eastern Gulf of Mexico provided by magnetic anomaly data: *Journal of Geophysical Research*, v. 99, p. 7161–7175, doi: 10.1029/93JB02570.
- Hawkesworth, C.J., Gallagher, K., Hergt, J.M., and McDermott, F., 1993, Trace element fractionation processes in the generation of island arc basalts, in Cox, K.G., et al., eds., Melting and melt movement in the Earth: Royal Society of London Philosophical Transactions, v. 342, p. 179–191, doi: 10.1098/rsta.1993.0013.
- Haxel, G.B., Anderson, T.H., Briske, J.A., Tosdal, R.M., Wright, J.E., and May, D.J., 2008, Late Jurassic igneous rocks in south-central Arizona and north central Sonora: Magmatic accompaniment of crustal extension, in Spencer, J.E., and Titley, S.R., eds., Ores and orogenesis: Circum-Pacific tectonics, geologic evolution, and ore deposits: Arizona Geological Society Digest 22, p. 333–335.
- Herrera-Soto, M.E., and Estavillo-González, C.F., 1991, Análisis estratigráfico y modelo de sedimentación en la Formación Todos Santos en el área del alto Uzpanapa-Matías Romero, Oaxaca: *Revista del Instituto Mexicano del Petróleo*, v. 22, p. 5–42.
- Iriondo, A., 2001, Proterozoic basements and their laramide juxtaposition in NW Sonora, Mexico: Tectonic constraints on the SW margin of Laurentia [Ph.D. thesis]: Boulder, University of Colorado, 222 p.
- Izaguirre-Pompa, A., 2009, El basamento Paleoproterozóico (~1.71–1.68 Ga) Yavapai en el área Mina La Herradura en el NW de Sonora: Sus implicaciones para el desarrollo del arco magmático continental Mesozoico-Cenozoico del NW de México [M.S. thesis]: Querétaro, Universidad Nacional Autónoma de México, 200 p.
- Jones, N.W., McKee, J.W., Anderson, T.H., and Silver, L.T., 1995, Jurassic volcanic rocks in northeastern Mexico: a possible remnant of a Cordilleran magmatic arc, in Jacques-Ayala, C., et al., eds., Studies on the Mesozoic of Sonora and adjacent areas: Geological Society of America Special Paper 301, p. 179–190, doi: 10.1130/0-8137-2301-9.179.
- Keppie, J.D., Dostal, J., Cameron, K.L., Solar, L.A., Ortega-Gutiérrez, F., and Lopez, R., 2003, Geochronology and geochemistry of Grenvillian igneous suites in the northern Oaxacan Complex, southern Mexico: tectonic implications: *Precambrian Research*, v. 120, p. 365–389, doi: 10.1016/S0301-9268(02)00166-3.
- Keppie, J.D., Dostal, J., Morman, N., Urrutia-Fucugauchi, J., and Grajales-Nishimura, M., 2010, Study of melt and clast of 546 Ma magmatic arc rocks in the Chicxulub

- breccia, northern Maya block, Mexico: Western limit of Ediacaran arc peripheral to northern Gondwana: International Geology Review, v. 1, p. 1–14; doi: 10.1080/00206810903545527.
- Krogh, T.E., Kamo, S.L., Sharpton, V.L., Marin, L.E., and Hildebrand, A.R., 1993, U-Pb ages of single shocked zircons linking distal K/T ejecta to the Chicxulub crater: Nature, v. 366, p. 731–734; doi: 10.1038/366731a0.
- López-Ramos, E., 1981, Paleogeografía y tectónica del mesozoico en México: Instituto de Geología, Universidad Nacional Autónoma de México, Revista, v. 5, p. 158–177.
- Marton, G., and Buffler, R.T., 1994, Jurassic reconstruction of the Gulf of Mexico basin: International Geology Review, v. 36, p. 545–586; doi: 10.1080/00206810940965475.
- Mauel, D.J., Lawton, T.F., Gonzalez Leon, C., Iriondo, A., Villasenor, A.B., and Amato, J.M., 2004, Late Jurassic stratigraphy, sedimentology, and geochronology of the Altar-Cucurpe Basin in the vicinity of Cucurpe, Sonora, northwestern Mexico; implications for Mesozoic tectonics of the southwestern North American margin: Geological Society of America Abstracts with Programs, v. 36, no. 5, p. 510.
- Mauel, D.J., Lawton, T.F., Gonzalez-Leon, C.M., Iriondo, A., and Amato, J.M., 2010, Stratigraphy and age of Upper Jurassic strata in North-central Sonora, Mexico: Southwestern Laurentian record of crustal extension and tectonic transition: Geosphere, v. 7, doi: 10.1130/GEO2006001.
- McCabe, C., van der Voo, R., and Urrutia-Fucugauchi, J., 1988, Late Paleozoic or early Mesozoic magnetizations in remagnetized Paleozoic rocks, State of Oaxaca, Mexico: Earth and Planetary Science Letters, v. 91, p. 205–213; doi: 10.1016/0012-821X(88)90162-8.
- McKee, J.W., Jones, N.W., and Anderson, T.H., 1988, Las Delicias Basin: a record of late Paleozoic arc volcanism in northeastern Mexico: Geology, v. 16, p. 37–40; doi: 10.1130/0091-7613(1988)016<0037:LDBARO>2.3.CO;2.
- Meneses-Rocha, J.J., 1985, Tectonic evolution of the strike-slip fault province of Chiapas, Mexico [M.S. thesis]: Austin, University of Texas at Austin, 315 p.
- Mixon, R.B., Murray, G.E., and Díaz-González, T.E., 1959, Age and correlation of Huizachal group (Mesozoic), State of Tamaulipas, Mexico: American Association of Petroleum Geologists Bulletin, v. 43, p. 757–771.
- Moecher, D.P., and Samson, S.D., 2006, Differential zircon fertility of source terranes and natural bias in the detrital zircon record: Implications for sedimentary provenance analysis: Earth and Planetary Science Letters, v. 247, p. 252–266; doi: 10.1016/j.epsl.2006.04.035.
- Mojica, J., Kammer, A., and Ujueta, G., 1996, El Jurásico del sector noroccidental de Suramérica y guía de la excursión al Valle Superior del Magdalena (Nov. 1–4/95), regiones de Payandé y Prado, Departamento del Tolima, Colombia: Geología Colombiana, v. 21, p. 3–40.
- Molina Garza, R.S., and Geissman, J.W., 1999, Paleomagnetic data from the Caborca Terrane, Mexico: implications for Cordilleran tectonics and the Mojave-Sonora megashare hypothesis: Tectonics, v. 18, p. 293–325; doi: 10.1029/1998TC900030.
- Molina Garza, R.S., Van der Voo, R., and Urrutia-Fucugauchi, J., 1992, Paleomagnetism of the Chiapas Massif, southern Mexico: evidence for rotation of the Maya Block and implications for the opening of the Gulf of Mexico: Geological Society of America Bulletin, v. 104, p. 1156–1168; doi: 10.1130/0016-7606(1992)104<1156:POTCMS>2.3.CO;2.
- Mori, L., Gómez-Tuena, A., Cai, Y., and Goldstein, S.L., 2007, Effects of prolonged flat subduction on the Miocene magmatic record of the central Trans-Mexican volcanic belt: Chemical Geology, v. 244, p. 452–473; doi: 10.1016/j.chemgeo.2007.07.002.
- Mori, L., Gómez-Tuena, A., Schaaf, P., Goldstein, S.L., Pérez-Arizu, O., and Solís-Pichardo, G., 2009, Lithospheric removal as a trigger for flood basalt magmatism in the Trans-Mexican volcanic belt: Journal of Petrology, v. 50, p. 2157–2186; doi: 10.1093/petrology/egp072.
- Movarec, D., 1983, Study of the Concordia fault system near Jericó, Chiapas, México [M.S. thesis]: Arlington, University of Texas, 148 p.
- Nourse, J.A., 1995, Jurassic-Cretaceous paleogeography of the Magdalena region, northern Sonora, and its influence on the positioning of Tertiary metamorphic core complexes, in Jacques-Ayala, C., et al., eds., Studies on the Mesozoic of Sonora and adjacent areas: Geological Society of America Special Paper 301, p. 59–78; doi: 10.1130/0-8137-2301-9.59.
- Nourse, J.A., Prewo, W.R., Iriondo, A., and Stahl, E.R., 2005, Contrasting Proterozoic basement complexes near the truncated margin of Laurentia, northwestern Sonora–Arizona international border region, in Anderson, T.H., et al., eds., The Mojave-Sonora megashare hypothesis: Development, assessment, and alternatives: Geological Society of America Special Paper 393, p. 123–182; doi: 10.1130/0-8137-2393-0.123.
- Ochoa-Camarillo, H.R., Buitrón, B.E., and Silva-Pineda, A., 1998, Contribución al conocimiento de la bioestratigrafía, paleoecología y tectónica del Jurásico (anticlinal de Huayacocotla) en la región de Molango, Hidalgo, Mexico: Revista Mexicana de Ciencias Geológicas, v. 15, p. 57–63.
- Pantoja Alor, J., 1963, A geological reconnaissance of the San Pedro del Gallo area, Durango, Mexico [M.S. thesis]: Tucson, University of Arizona, 163p.
- Pérez-Gutiérrez, R., Solari, L.A., Gómez-Tuena, A., and Valencia, V.A., 2009, El terreno Cuicateco: ¿cuenca oceánica con influencia de subducción del Cretácico Superior en el sur de México? Nuevos datos estructurales, geoquímicos y geocronológicos: Revista Mexicana de Ciencias Geológicas, v. 26, p. 222–242.
- Pindell, J.L., and Dewey, J.F., 1982, Permo-Triassic reconstruction of western Pangea and the evolution of the Gulf of Mexico/Caribbean region: Tectonics, v. 1, p. 179–211; doi: 10.1029/TC001i002p00179.
- Pindell, J.L., Cande, S.C., Pitman, W.C., III, Rowley, D.B., Dewey, J.F., LaBrecque, J.L., and Haxby, W.F., 1988, A plate-kinematic framework for models of Caribbean evolution: Tectonophysics, v. 155, p. 121–138; doi: 10.1016/0040-1951(88)90262-4.
- Pindell, J., Kennan, L., Stanek, K.P., Maresch, W.V., and Draper, G., 2006, Foundations of Gulf of Mexico and Caribbean evolution: Eight controversies resolved: Geologica Acta, v. 4, p. 303–341.
- Restrepo-Pace, P.A., Ruiz, J., Gehrels, G., and Cosca, M., 1997, Geochronology and Nd isotopic data of Grenville-age rocks in the Colombian Andes: New constraints for Late Proterozoic–early Paleozoic paleocontinental reconstructions of the Americas: Earth and Planetary Science Letters, v. 150, p. 427–441; doi: 10.1016/S0012-821X(97)00091-5.
- Ross, M.I., and Scotese, C.R., 1988, A hierarchical tectonic model of the Gulf of Mexico and Caribbean region: Tectonophysics, v. 155, p. 139–168; doi: 10.1016/0040-1951(88)90263-6.
- Rubio-Cisneros, I.I., and Lawton, T.F., 2010, Detrital zircon U-Pb ages of sandstones in continental red beds at Valle de Huizachal, Tamaulipas, NE Mexico: Record of Early–Middle Jurassic arc volcanism and transition to crustal extension: Geosphere, v. 7, doi: 10.1130/GES00567.1.
- Rueda-Gaxiola, J., 1998, El origen del Golfo de México y de sus subcuenca petroleras mexicanas, con base en la palinología de lechos rojos: Revista Mexicana de Ciencias Geológicas, v. 15, p. 78–86.
- Salvador, A., 1987, Late Triassic–Jurassic paleogeography and origin of Gulf of Mexico Basin: American Association of Petroleum Geologists Bulletin, v. 71, p. 419–451.
- Scott, E., and Peel, F., 2001, Deep water Gulf of Mexico sea floor features revealed through 3D seismic: Offshore Technology Conference Proceedings, v. 33, p. 239–248; doi: 10.4043/12961-MS.
- Silva-Romo, G., Arellano Gil, J., Mendoza Rosales, C., and Nieto Obregón, J., 2000, A submarine fan in the Mesa Central, Mexico, in Centeno García, E., et al., eds., Geologic evolution of the Guerrero terrane, western Mexico: Journal of South American Earth Sciences, v. 13, p. 429–442; doi: 10.1016/S0895-9811(00)00034-1.
- Solari, L.A., Dostal, J., Ortega-Gutiérrez, F., and Keppie, D., 2001, The 275 Ma arc-related La Carbonera stock in the northern Oaxacan Complex of southern Mexico: U-Pb geochronology and geochemistry: Revista Mexicana de Ciencias Geológicas, v. 18, p. 149–161.
- Solari, L.A., Ortega-Gutiérrez, F., Elías-Herrera, M., Gómez-Tuena, A., and Schaaf, P., 2009, Refining the age of magmatism in the Altos Cuchumatanes, western Guatemala, by LA-ICPMS, and tectonic implications: International Geology Review, v. 1, p. 1–22; doi: 10.1080/00206810903216962.
- Stacey, J.S., and Kramers, J.D., 1975, Approximation of terrestrial lead isotope evolution by a two-stage model: Earth and Planetary Science Letters, v. 26, p. 207; doi: 10.1016/0012-821X(75)90088-6.
- Steiner, M.B., and Walker, J.D., 1996, Late Silurian plutons in Yucatan: Journal of Geophysical Research, v. 101, p. 17,727–17,735; doi: 10.1029/96JB00174.
- Stern, R.J., and Dickinson, W.R., 2009, The Gulf of Mexico: A Late Jurassic back-arc basin: Geological Society of America Abstracts with Programs, v. 41, no. 2, p. 36.
- Stern, R.J., and Dickinson, W.R., 2010, The Gulf of Mexico is a Jurassic back-arc basin: Geosphere, v. 6, p. 739–754; doi: 10.1130/GES00585.1.
- Sun, S.S., and McDonough, W.F., 1989, Chemical and isotopic systematics of oceanic basalts: implications for mantle composition and processes, in Saunders, A.D., and Norry, M.J., eds., Magmatism in the ocean basins: Geological Society of London Special Publication 42, p. 313–345; doi: 10.1144/GSL.SP.1989.042.01.19.
- Torres-Vargas, R., Ruiz, J., Patchett, P.J., and Grajales, J.M., 1999, Permo-Triassic continental arc in eastern Mexico: tectonic implications for reconstructions of southern North America, in Bartolini, C., et al., eds., Mesozoic sedimentary and tectonic history of north-central Mexico: Geological Society of America Special Paper 340, p. 191–196; doi: 10.1130/0-8137-2340-X.191.
- Vinegar-Osorio, F., 1971, Age and evolution of salt basins of southeastern Mexico: American Association of Petroleum Geologists Bulletin, v. 55, p. 478–494.
- Walker and Geissman, compilers, 2009, Geologic time scale: Boulder, Colorado, Geological Society of America, doi: 10.1130.2009.CTS004R2C.
- Weber, B., and Kohler, H., 1999, Sm-Nd, Rb-Sr and U-Pb geochronology of a Grenville terrane in southern Mexico: Origin and geologic history of the Guichicovi Complex: Precambrian Research, v. 96, p. 245–262, doi: 10.1016/S0301-9268(99)00012-1.
- Weber, B., Cameron, K.L., Osorio, M., and Schaaf, P., 2005, A Late Permian tectonothermal event in Grenville crust of the southern Maya terrane; U-Pb zircon ages from the Chiapas Massif, southeastern Mexico: International Geology Review, v. 47, p. 509–529; doi: 10.2747/0020-6814.47.5.509.
- Weber, B., Schaaf, P., Valencia, V.A., Iriondo, A., and Ortega-Gutiérrez, F., 2006, Provenance ages of late Paleozoic sandstones (Santa Rosa Formation) from the Maya Block, SE Mexico: implications on the tectonic evolution of western Pangea: Revista Mexicana de Ciencias Geológicas, v. 23, p. 262–276.
- Weber, B., Iriondo, A., Premo, W.R., Hecht, L., and Schaaf, P., 2007, New insights into the history and origin of the southern Maya block, SE México: U-Pb SHRIMP zircon geochronology from metamorphic rocks of the Chiapas massif: International Journal of Earth Sciences, v. 96, p. 253–269; doi: 10.1007/s00531-006-0093-7.
- Weber, B., Valencia, V.A., Schaaf, P., Pompa-Mera, V., and Ruiz, J., 2008, Significance of provenance ages from the Chiapas Massif Complex (southeastern Mexico): Redefining the Paleozoic basement of the Maya block and its evolution in a Peri-Gondwanan Realm: Journal of Geology, v. 116, p. 619–639; doi: 10.1086/591994.
- Winker, C.D., and Buffler, R.T., 1988, Paleogeographic evolution of early deep-water Gulf of Mexico and margins, Jurassic to Middle Cretaceous (Comanchean): American Association of Petroleum Geologists Bulletin, v. 72, p. 318–346.

MANUSCRIPT RECEIVED 31 MARCH 2010

REVISED MANUSCRIPT RECEIVED 15 JUNE 2010

MANUSCRIPT ACCEPTED 7 JULY 2010